

Spectral properties of transition metal pnictides and chalcogenides: angle-resolved photoemission spectroscopy and dynamical mean field theory

Ambroise van Roekeghem

Centre de Physique Théorique, Ecole Polytechnique, CNRS, Université Paris-Saclay, 91128 Palaiseau, France

Beijing National Laboratory for Condensed Matter Physics, and Institute of Physics, Chinese Academy of Sciences, Beijing 100190, China

Pierre Richard, Hong Ding

Beijing National Laboratory for Condensed Matter Physics, and Institute of Physics, Chinese Academy of Sciences, Beijing 100190, China

Collaborative Innovation Center of Quantum Matter, Beijing, China

Silke Biermann

Centre de Physique Théorique, Ecole Polytechnique, CNRS, Université Paris-Saclay, 91128 Palaiseau, France

Collège de France, 11 place Marcelin Berthelot, 75005 Paris, France

European Theoretical Synchrotron Facility, Europe

Abstract

Electronic Coulomb correlations lead to characteristic signatures in the spectroscopy of transition metal pnictides and chalcogenides: quasi-particle renormalizations, lifetime effects or incoherent bad metallic behavior above relatively low coherence temperatures are measures of many-body effects due to local Hubbard and Hund's couplings. We review and compare the results of angle-resolved photoemission spectroscopy experiments (ARPES) and of combined density functional dynamical mean field theory (DFT+DMFT) calculations. We emphasize the doping-dependence of the quasi-particle mass renormalization and coherence properties.

Keywords: Electronic Coulomb correlations, correlation strength, angle-resolved photoemission spectroscopy, electronic structure calculations, dynamical mean field theory, transition metal pnictides and chalcogenides, Hund's metals, doping-dependent coherence, spin-freezing, superconducting gap symmetry

1. Introduction

Angle-resolved photoemission spectroscopy (ARPES) is a powerful tool to probe the electronic properties of materials. It allows for a measurement of the momentum-resolved spectral function, providing crucial information on the Fermi surface, the quasi-particle dispersions, or even the momentum-resolved magnitude of the superconducting gap. It can also give insights into the orbital characters of the electronic states through the use of polarized light, core and plasmon excitations, and some clues about the lifetime of quasiparticles – though the latter point is more delicate since the measurements can be influenced by the sample quality or other extrinsic limitations. In the following, we will focus on measurements in the

Email address: vanroeke@cph.t.polytechnique.fr (Ambroise van Roekeghem)

paramagnetic normal state, except for Section 5 where we summarize recent work on measurements of the superconducting gap.

This review is organized as follows: in Sections 2 and 3 we give brief introductions to the basics of photoemission spectroscopy and dynamical mean field based electronic structure calculations respectively. Section 4 provides an overview over the spectral properties of transition metal pnictide and chalcogenides from a combined experimental and theoretical point of view. Section 5 is devoted to measurements of the superconducting gap, while Section 6 summarizes recent theoretical advances.

2. Angle-resolved photoemission spectroscopy

2.1. Introduction

Photoemission spectroscopy, also called photoelectron spectroscopy, is a technique based on the photoelectric effect [1]. A light source is used to produce photons of a given energy, which are sent on a sample with a chosen incidence. An electron of the sample can then absorb a photon of the incident beam and escape with a maximum energy $E = \hbar\omega - \phi$ with ϕ the workfunction of the material. By collecting those electrons and analyzing their energies and wave vectors, one obtains information about the electronic structure of the material, such as a direct visualization of the quasiparticle dispersions and of the Fermi surface (for a comprehensive book, see e.g. Ref. [2], for an introduction, see e.g. Ref. [3, 4]).

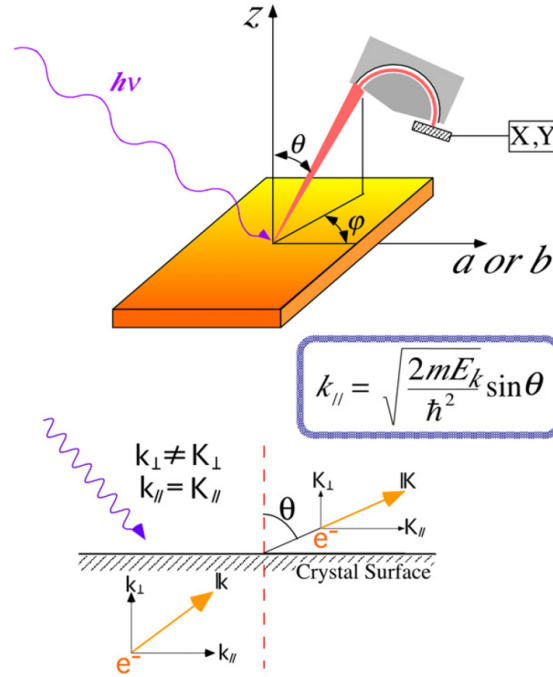


Figure 1: Principles of an angle-resolved photoemission experiment (reprinted with permission from Ref. [5], copyright ©(2011) by IOP Publishing).

The photoemission process is often interpreted within the three-step model, in which the electron is excited from an initial state to a final state, then travels to the surface, and finally escapes from the solid. Fundamentally, the analysis of the photoemission spectrum is a many-body problem, for the escape of an electron leaves the solid in an excited state that may involve several electrons. Another description making use of fewer approximations is the one-step model, in which the photoemission process is described as an optical transition between a ground-state many-body wave function involving N electrons and an excited wave function involving $N-1$ electrons and an escaping plane wave. The photocurrent is described within

the sudden approximation, which states that the creation of the photohole is instantaneous and that there is no interaction between the escaped electron and the remaining system. The photocurrent in the three-step model is proportional to the probability of transition between the ground state and all final states. For a given final state it is determined by Fermi's golden rule:

$$w_{fi} = \frac{2\pi}{\hbar} | \langle \psi_f^N | H^{int} | \psi_i^N \rangle |^2 \delta(E_f^N - E_i^N - h\nu) \quad (1)$$

In the sudden approximation, $\langle \psi_f^N | H^{int} | \psi_i^N \rangle = \langle \phi_f^k | \tilde{H}^{int} | \phi_i^k \rangle \langle \psi_f^{N-1} | c_k | \psi_i^N \rangle$, where ϕ^k is a one-electron wave function.

This factorization is valid in the limit of infinite photon energy, and is used as an approximation in practice. It has been argued that the adiabatic to sudden transition takes place at a very large photon energy – of the order of the keV – when many-body effects like core electron - plasmon interaction take place, while smaller energies are required in the case of a localized system (see for instance [6, 7]). Still, most of the ARPES experimental analysis is nowadays done within the sudden approximation. For a pedagogical discussion of effects beyond the sudden approximation we refer the reader to Ref. [8]. A DMFT-based approach in the framework of the one-step model has been worked out in Ref. [9].

Summing over all possible excited final states ψ_e^{N-1} with energy E_e^{N-1} and writing $\langle \phi_f^k | \tilde{H}^{int} | \phi_i^k \rangle = M_{f,i}^k$ the one-electron dipole matrix element, we see that the probability of detecting an electron with wave vector k and energy E_{kin} is proportional to:

$$I(k, E_{kin}) \propto \sum_{f,i} |M_{f,i}^k|^2 \sum_e | \langle \psi_e^{N-1} | c_k | \psi_i^N \rangle |^2 \delta(E_{kin} + E_e^{N-1} - E_i^N - h\nu) \quad (2)$$

Finally, we take into account the resolution of the experiment and the effect of temperature and see that the photocurrent is proportional to the spectral function $A(k, \omega) = \sum_e | \langle \psi_e | c_k | \psi_0 \rangle |^2 \delta(\omega + E_e^{(N-1)} - E_0^{(N)})$, $\omega < 0$:

$$I(k, \omega) = I_0(k, \nu, \vec{A}) A(k, \omega) f(\omega) * R(k, \omega) \quad (3)$$

with R being the resolution function of our ARPES experiment, f the Fermi function, and I_0 a prefactor depending on one-electron matrix elements. ω is the energy of electrons in the solid with respect to the Fermi level. The spectral function is a quantity we calculate directly from first principles using Dynamical Mean Field Theory (DMFT), see Section 3 and Ref. [10] for an overview of calculations of spectral properties for oxide materials. Hence, those two techniques are an ideal match to compare experimental and theoretical results. However, due to the small mean free path of electrons at the kinetic energies we consider [11], ARPES is a surface probe. This can further complicate the interpretation of the results if the surface electronic structure is different from the bulk. Furthermore, the component of the wave vector perpendicular to the plane is not conserved during the photoemission process, only the in-plane component is (see Figure 1).

Under the assumptions of an independent particle picture, the sudden approximation and the three-step model, one can directly study the momentum-resolved band-structure of the solid. Under these conditions, one can also extract the perpendicular component of the wave vector: using a nearly-free electron model for the final state, one has the dispersion:

$$k_{\perp} = \frac{\sqrt{2m}}{\hbar} \sqrt{E_{kin} \cos^2 \theta + V_0} \quad (4)$$

with θ the polar angle as in Figure 1 and V_0 the inner potential, which depends on the material considered and represents the bottom of a free-electron-like band dispersion for the final state with respect to the vacuum level. In practice, to estimate V_0 one can vary the photon energy – which is possible using synchrotron light – and observe a periodic dispersion of the band structure.

In recent years, important progress has been made both on the detection setup and on the light sources. At present, ARPES can provide a resolution of the order of the meV and access a large temperature range,

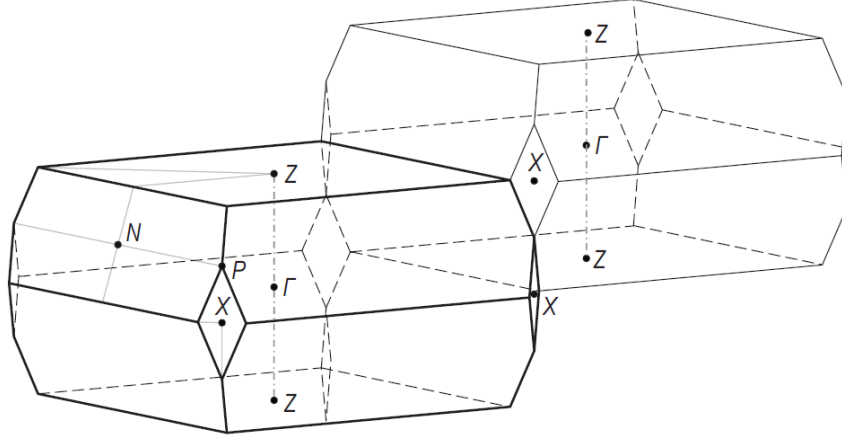


Figure 2: Body-centered tetragonal first and second Brillouin zone (reprinted with permission from Ref. [18]).

even below 1K. Using a laser as the light source allows for a very fine resolution and a higher sensitivity to the bulk but limits the momentum and energy range that can be accessed due to the small difference between the photon energy and the workfunction. In contrast, synchrotron light offers the possibility to tune the photon energy and thus to select the wave number perpendicular to the sample surface, or to use soft x-rays to also probe the bulk of the crystal and a large area of the momentum space. The versatility of this technique is also exceptional, since it can be used on materials synthesized in situ or on a microscopically defined area, and with spin- or time-resolution.

An obvious limitation is of course that the information provided by ARPES is limited to the occupied part of the spectrum. Inverse photoemission techniques such as Bremsstrahlung isochromate spectroscopy (BIS) on the other hand suffer from generally much lower resolution, due to the weak cross section of the electron addition process [2]. Pump-probe techniques where the electronic system is excited by a pump pulse before being probed by ARPES provide a promising alternative. Assuming that the main effect of the pump pulse is to heat the electronic system to a high effective temperature, one obtains information on empty states within the corresponding energy range [12, 13]. We note, however, that the conditions of validity of such an assumption are a largely open question, since in general one faces a truly non-equilibrium situation invalidating the notion of effective electronic temperature and making the interpretation of the experiment much more involved. In practical applications to iron pnictide compounds [14, 15, 16, 17] the main interest in applying pump-probe spectroscopy has rather been lying in the possibility of analyzing different relaxation processes, giving information e.g. on electron-phonon coupling.

2.2. Conventions and notations

Iron pnictides in the tetragonal, paramagnetic phase present two different crystal structures: while the 11, 111 and 1111 have simple tetragonal stacking with $P4/nmm$ space group, the 122 family crystallizes in the body-centered tetragonal ThCr_2Si_2 -type crystal structure ($I4/mmm$ space group), in which the two arsenic atoms of different layers are on top of each other – the layers are translated before they are stacked on top of each other. The three-dimensional Brillouin zone of this family is represented in Figure 2, with the crystallographic notations for the high-symmetry points. The literature on iron pnictides can be confusing because high-symmetry points are often denominated differently, due to the different space groups and authors considering so-called “one-Fe” or “two-Fe” unit cells – that is to say, a Brillouin zone that ignores the translation-breaking potential created by the alternating positions of the arsenic atoms above and below the iron plane, or one which takes it into account. In particular, the crystallographic X point in the 122 Brillouin zone is often named M in the “one-Fe” notation. In contrast, the corresponding point of the electronic structure of the $P4/nmm$ Brillouin zone is also named M in the crystallographic conventions.

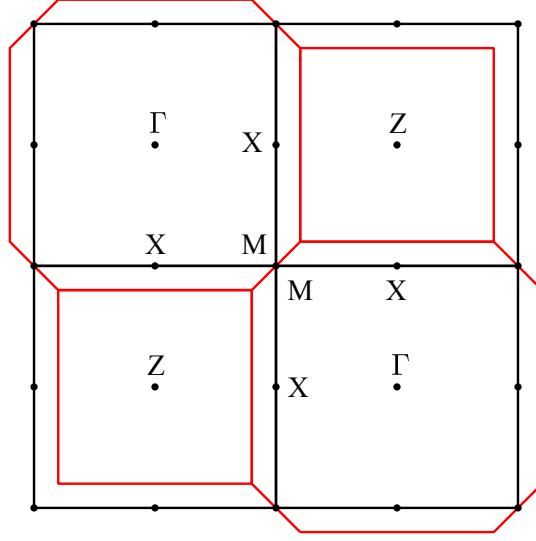


Figure 3: Cut of the body-centered tetragonal Brillouin zones in the $k_z = 0$ plane (red) along with our choice of notations for the high-symmetry points (black). The simple tetragonal Brillouin zones would correspond to black lines, but the Z points would be replaced by Γ points.

In our case and for practical purposes, we will define our points for the body-centered tetragonal Brillouin zone as in Figure 3, which shows a cut of the Brillouin zone at $k_z = 0$. One can see that our X point is actually not a high symmetry point along the $\Gamma X Z$ direction – where there is no high symmetry point a priori. On the other hand, M is a well defined high symmetry point on both $\Gamma M \Gamma$ and $Z M Z$ directions. Interestingly, in the simple tetragonal Brillouin zone X becomes a high symmetry point along the ΓX direction, for the Z points of Figure 3 would be replaced by Γ points. This choice allows for a relative uniformity of notations within the different pnictides families, and is in line with the more often encountered “one-Fe unit cell” notations.

2.3. Orbital characters and matrix elements

A common procedure in ARPES to obtain information about the orbital characters of electronic states consists in using different light polarizations to highlight or filter certain symmetries. The matrix element $I_0(k, \nu, \vec{A})$ is proportional to:

$$I_0(k, \nu, \vec{A}) \propto | \langle \phi_k^f | \vec{\epsilon} \cdot \vec{x} | \phi_k^i \rangle |^2 \quad (5)$$

with $|\phi_k^f\rangle$ and $|\phi_k^i\rangle$ the final and initial states respectively and $\vec{\epsilon}$ a unit vector along the direction of the polarization of the vector potential \vec{A} . The principle is then to find a mirror plane in which we detect the photoelectrons that allows us to classify states into even or odd symmetry with respect to this plane. In that geometry, the final state has to be even to be detected, and so does $\vec{\epsilon} \cdot \vec{x} | \phi_k^i \rangle$ in order for the matrix element to be non-zero. Finally, if $\vec{\epsilon}$ is in the mirror plane (p polarization) we obtain that $|\phi_k^i\rangle$ has to be even, and if $\vec{\epsilon}$ is perpendicular to the plane (s polarization) $|\phi_k^i\rangle$ has to be odd.

However, in iron pnictides the problem is more complicated. Due to the fact that the arsenic position is alternating above and below the iron plane, creating a 2-Fe unit cell, there is no such mirror plane containing the ΓM direction. Still, a possibility to attribute symmetries to the electronic states is to consider this alternating position of As as a small perturbing potential that breaks the translational symmetry and to analyze the band structure as a superposition of a “main” in-phase band structure in the sense of the 1-Fe unit cell and of the corresponding out-of-phase folded band structure [20, 19]. The symmetry of the

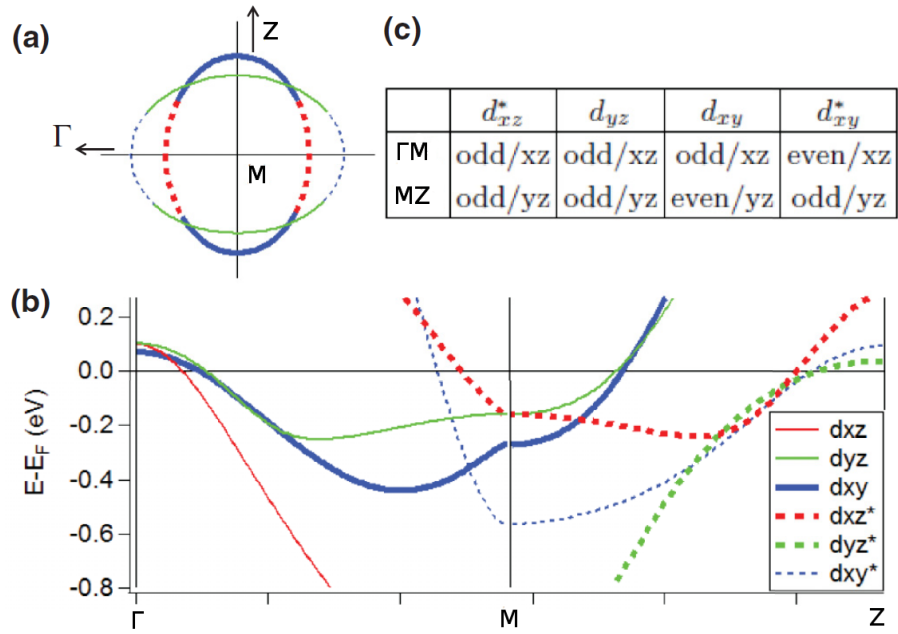


Figure 4: Effect of the 2-Fe unit cell on matrix elements

(a) Sketch of the bands forming the electron pockets. Solid and dotted lines represent the in-phase and out-of-phase orbitals. Colors indicate the main orbital character. (b) Sketch of the dispersion of the different bands along the path Γ MZ (in the $k_z = 0$ plane). The color sketches the main orbital character, although there may be hybridization with other orbitals. (c) Symmetries of the different bands forming the electron pockets at M. (Adapted with permission from Ref. [19] (copyright ©(2012) by The American Physical Society), using the notations of Figure 3)

electronic states is found to be different due to the alternating arsenic position. Furthermore, a second effect appears, due to the fact that the final state – close to a free-electron state – is not sensitive to the potential breaking the translational symmetry. As a consequence, the spectral weight is different in the first and second Brillouin zones, with the bands originating mainly from folding having little spectral weight in the first Brillouin zone. Those results are summarized in Figure 4, in particular for the electron pockets around the M point, which are the most impacted.

3. First-principles approaches to spectral properties of transition metal pnictide materials

When studying the electronic properties of materials, theories assuming a single-particle band picture where the electrons are considered to be non-interacting fermions in an effective periodic potential often produce remarkable results. In fact, for ground state properties the Hohenberg-Kohn theorem of Density Functional Theory guarantees the exact solution to be of this form, and Density Functional Theory – even though in practice using approximations to the exact functional – has been able to produce *ab initio* quantitative predictions for many chemical and physical systems [21]. However, care is in order when dealing with excited state properties where the Kohn-Sham band structure of DFT is not *a priori* a reasonable approximation. This is intrinsically true for the photoemission spectrum where effects beyond the band picture are expected and found. In order to arrive at a theoretical description that incorporates those into the *ab initio* description one borrows concepts from many-body theory, originally developed for lattice models of correlated fermions.

The key phenomenon modeled in interacting fermionic lattice models is the competition between the tendency to delocalization of the electrons driven by the corresponding lowering of the kinetic energy and local Coulomb interactions counteracting this delocalization. The most simple model – but containing very rich physics – was introduced by J. Hubbard [22, 23]. The idea is to include correlations in the original Hamiltonian by adding a Coulomb repulsion when several electrons are on the same atomic site. While the model was initially introduced in an *ad hoc* manner, nowadays, this interaction U between two electrons can actually be evaluated, for instance using the constrained-Random Phase Approximation (cRPA) [24]: with χ the wave function associated to the considered atomic level on the site R ,

$$U \sim \int dr dr' |\chi_R(r)|^2 W^r(r - r') |\chi_R(r')|^2$$

where W^r is a partially screened interaction between electrons. For more details on the calculation of U and of its frequency dependence in iron pnictides, see e.g. Ref. [25, 26, 27, 28].

In the single-orbital case at zero temperature the Hubbard U and the hopping terms are the only energy scales of the system. The physics is then simply determined by the competition between two phenomena: the electronic correlations introduced by U which tend to localize the electrons and the kinetic delocalization characterized by the hopping amplitudes. By tuning the ratio U/W , with W the bandwidth, one can then go all the way from the weak coupling (band) limit to the strong coupling (atomic) limit. Among compounds with partially filled $3d$ or $4f$ shells there are numerous examples of materials in the intermediate regime, where spectra are not well-described by the single-particle density of states nor solely consist of Hubbard bands but exhibit a renormalized quasi-particle peak accompanied by incoherent higher-energy excitations.

As discussed in Section 4, iron pnictides are in the intermediate regime where it is necessary to use a theory able to probe both strongly and weakly correlated regimes, such as Dynamical Mean Field Theory (DMFT), even though the multiorbital nature of the systems brings in additional interesting physics: the five $3d$ orbitals of the transition metal have a total bandwidth of about 5 eV within DFT, to be compared to a U of about 3 eV. In this – *a priori* moderately correlated – regime, the actual correlation strength is tuned by the suppression of screening channels due to Hund’s rule: the Coulomb cost for two electrons with anti-parallel spins is larger than the one for two electrons with parallel spins, since in the latter case the Pauli principle keeps the electrons apart. This intra-atomic exchange, the Hund’s rule coupling J , leads to most interesting multiorbital physics in this class of compounds [29, 30, 31].

Over the last decades, DMFT has been at the origin of impressive success in providing us with a qualitative understanding but also quantitative spectral functions directly comparable to experiments. We present

below a summary of the basic principles of DMFT (for extensive reviews, see [32, 33, 34, 35, 36, 37]) and of its combination with DFT for the case of transition-metal pnictides.

3.1. Combination of DFT and DMFT

The idea of “DFT+DMFT” is to combine the one-particle Hamiltonian from DFT with an improved description of a selection of states corresponding to orbitals of limited spatial extension, the “correlated states”, within DMFT [38, 39]. While modern implementations [40, 41] have become increasingly sophisticated, to first approximation, one can understand DFT+DMFT as the solution of a multi-orbital Hubbard model, the parameters of which stem from DFT. The DFT+DMFT Hamiltonian is then written as:

$$H^{DFT+DMFT} = H^{DFT} + H^{int} + H^{DC} \quad (6)$$

Here H^{DFT} corresponds to the one-particle Hamiltonian obtained by Density Functional Theory:

$$H^{DFT} = \sum_{i,j,\sigma,m} h_{m_1 m_2}^{ij} c_{i m_1 \sigma}^\dagger c_{j m_2 \sigma} \quad (7)$$

where c^\dagger and c are creation and annihilation operators, i and j different sites of the crystal, m represent different orbitals, σ is the spin and h is the Hamiltonian.

H^{int} corresponds to the interacting Hamiltonian within the low-energy model that is used to describe the electronic correlations:

$$H^{int} = \frac{1}{2} \sum_i \sum_{(m_1 \in d, \sigma) \neq (m_2 \in d, \sigma')} U_{m_1 \sigma m_2 \sigma'} n_{i m_1 \sigma} n_{i m_2 \sigma'} \quad (8)$$

Here the Hamiltonian includes only density-density interactions for practical reasons, but it can be generalized to be rotationally invariant. We note that in practice the full matrix $U_{m_1 \sigma m_2 \sigma'}$ can be parametrized using a set of three Slater integrals F^0 , F^2 , F^4 and can also depend on the frequency ω [25, 27].

Finally, H^{DC} is the double-counting Hamiltonian chosen such as to avoid double counting of contributions taken into account both in H^{DFT} and H^{int} .

3.2. Principles of Dynamical Mean Field Theory

In a few words, DMFT consists in replacing the lattice problem by a single site coupled to a bath, thus making a local approximation in space. The consequence is that the resulting many-body self-energy does not have momentum-dependence, but dynamical quantum fluctuations are fully included: the occupation of the single-site varies as electrons hop to the bath or from the bath to the site. This process is schematically represented on Figure 5.

In practice, a DMFT calculation is a two-step procedure iterated until self-consistency. The first is the mapping of the lattice model onto the effective auxiliary quantum impurity problem. The latter is characterized by the local Hubbard interaction, and a bath propagator describing hopping between site and bath in the absence of interactions. It can be thought of as a coupling between the non-interacting bath states l (of energy ϵ_l) and the impurity site by transition terms V_l . The creation and annihilation operators on the impurity are written c^\dagger and c respectively, while the corresponding operators for the bath are written a^\dagger and a . $n = c^\dagger c$ is the number of electrons on the impurity. We can decompose the Hamiltonian into three parts. One is related to the bath, another to the impurity, and the third one to the coupling between the bath and the impurity:

$$H_{AIM} = H_{bath} + H_{atom} + H_{coupling} \quad (9)$$

with

$$H_{atom} = \frac{1}{2} \sum_{(m_1, \sigma) \neq (m_2, \sigma')} U_{m_1 \sigma m_2 \sigma'} n_{m_1 \sigma} n_{m_2 \sigma'} + \sum_{m, \sigma} (\epsilon_{m, \sigma} - \mu) n_{m, \sigma}$$

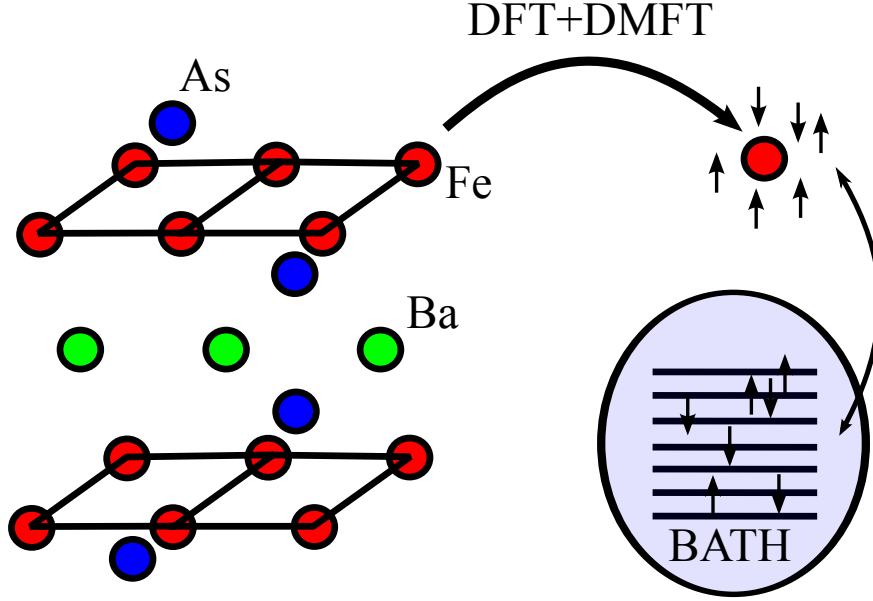


Figure 5: Representation of the treatment of a 122 iron pnictide by DFT+DMFT. The dynamical mean field approximation allows to map the crystal onto a problem of one atom exchanging electrons with a bath, while the Wannier orbitals and the free-electron-like hopping probabilities and electronic energies are calculated from the density functional theory energy bands.

$$H_{coupling} = \sum_{l,m,\sigma} V_{lm\sigma} (a_{l,\sigma}^\dagger c_{m,\sigma} + c_{m,\sigma}^\dagger a_{l,\sigma})$$

$$H_{bath} = \sum_{l,\sigma} \epsilon_l a_{l,\sigma}^\dagger a_{l,\sigma}$$

As in any mean field theory, a self-consistency condition is needed to related the auxiliary problem to the original one. In DMFT, one imposes that the local Green's function of the lattice, defined as the sum over the momentum k of the momentum-resolved Green's functions written in a localized basis set, is equal to the Green's function of the local model.

Actually, this Green's function of the impurity model only depends on a hybridization function Δ which integrates all the degrees of freedom of the bath:

$$\Delta_m(i\omega_n) = \sum_l \frac{V_{lm}^2}{i\omega_n - \epsilon_l}$$

through the formalism of an effective action S_{eff} :

$$S_{eff} = - \int_0^\beta d\tau \int_0^\beta d\tau' \sum_{m,\sigma} c_{m,\sigma}^\dagger(\tau) \mathcal{G}_{0m\sigma}^{-1}(\tau - \tau') c_{m,\sigma}(\tau') + \frac{1}{2} \sum_{(m_1,\sigma) \neq (m_2,\sigma')} U_{m_1\sigma m_2\sigma'} \int_0^\beta d\tau n_{m_1,\sigma}(\tau) n_{m_2,\sigma'}(\tau)$$

in which the Weiss dynamical mean field \mathcal{G}_0 is defined as:

$$\mathcal{G}_0^{-1}(i\omega_n) = i\omega_n + \mu - \epsilon_0 - \Delta(i\omega_n)$$

This means that the impurity model is fully described by the effective field \mathcal{G}_0 and the Hubbard U .

If we assume that we can solve the model and find the associated Green's function G_{imp} , we then get access to the impurity model self energy:

$$\Sigma_{imp}(i\omega_n) \equiv \mathcal{G}_0^{-1}(i\omega_n) - G_{imp}^{-1}(i\omega_n)$$

We now make the DMFT approximation: identifying the impurity model self-energy with the lattice self-energy,

$$\Sigma(k, i\omega_n) \simeq \Sigma_{imp}(i\omega_n) \quad (10)$$

In so doing, we loose the non-local components of the self-energy (there is no momentum dependence of the self-energy any more) and approximate the local component by that of the effective local problem.

Consequently, the lattice local Green's function G_{local} is computed as:

$$G_{local}^{m\sigma}(i\omega_n) = \int dk G_{local}^{m\sigma}(k, i\omega_n) = \left(\int dk [i\omega_n + \mu - \Sigma_{imp}(i\omega_n) - H(k)]^{-1} \right)^{m\sigma} \quad (11)$$

The self-consistency condition (the correspondence between the lattice and the model) requires this new local Green's function to equal the impurity one ($G_{local} = G_{imp}$), that is, it can be used to update the dynamical mean field through the Dyson equation:

$$\mathcal{G}_0^{-1} = G_{local}^{-1} + \Sigma$$

This defines a new local problem that has to be solved, and the cycle is iterated until the Green's function, Weiss field and self-energy are converged.

In summary, the Green's function of an electron in the bath is self-consistently determined, such that the impurity's Green's function is exactly equal to the local Green's function of the lattice – within the DMFT approximation $\Sigma(k, i\omega_n) \simeq \Sigma(i\omega_n)$.

The technical challenge is the resolution of the impurity model, which is computationally demanding but at present is relatively accessible, notably thanks to the implementation of efficient Monte Carlo algorithms for Anderson impurity problems [42].

3.3. Survival Kit: Properties of the Spectral Function

In this section, we provide a few useful relations concerning the one-particle spectral function. For simplicity, we consider the single-orbital case.

Let us suppose that we have a spectral function $A(k, \omega)$, which measures the probability of extracting an electron of momentum k and energy ω [43] during the (direct/inverse) photoemission process. In the case where there is only one energy associated to each momentum, such as for a free particle, $A(k_0, \omega) = \delta(\omega(k_0))$ (k_0 being fixed). However, in interacting systems, $A(k_0, \omega)$ displays quasi-particle peaks that have a certain width (corresponding to the inverse quasi-particle lifetime) and high-energy features can be generated in addition. Still, by construction $A(k_0, \omega) \geq 0$ and the spectral function is normalized:

$$\int_{-\infty}^{+\infty} \frac{d\omega}{2\pi} A(k_0, \omega) = 1 \quad (12)$$

(Of course, the specific value of the normalization is a choice. Here we normalize per spin and per orbital. Another possibility would be to normalize to the total number of states (summing over orbitals and spin).)

This probability allows us to compute physical quantities, as it codes the relation between momentum and energy. As a simple example, we can mention the total number of electrons with momentum k :

$$n_k = \int_{-\infty}^{+\infty} \frac{d\omega}{2\pi} n_F(\omega) A(k, \omega) \quad (13)$$

Summing $A(k, \omega)$ over momentum distribution gives the k-integrated spectral function of the interacting system, that is to say the density of electrons we can extract from the system by employing a certain energy, regardless of their momentum. This quantity is thus useful for comparison to angle-integrated photoemission.

The spectral function can be obtained from the Green's function as:

$$A(k, \omega) = -2\text{Im}G_{ret}(k, \omega) \quad (14)$$

Inversely, we can also express the Green's functions from the spectral function via a Hilbert transformation:

$$\begin{aligned} G(k, i\omega) &= \int_{-\infty}^{+\infty} \frac{d\omega'}{2\pi} \frac{A(k, \omega')}{i\omega - \omega'} \\ G_{ret}(k, \omega) &= \int_{-\infty}^{+\infty} \frac{d\omega'}{2\pi} \frac{A(k, \omega')}{\omega - \omega' + i0^+ \text{sign}(\omega')} \end{aligned}$$

Finally, we can express the spectral function directly in terms of the self-energy:

$$A(k, \omega) = \frac{-2\text{Im}\Sigma_{ret}(k, \omega)}{[\omega - \epsilon_k - \text{Re}\Sigma_{ret}(k, \omega)]^2 + [\text{Im}\Sigma_{ret}(k, \omega)]^2} \quad (15)$$

We now turn to a discussion of the link of the spectral function A to ARPES experiments. Indeed, the spectral function can be understood as an overlap between the ground state with N electrons and excited states with $N-1$ or $N+1$ electrons [43]:

$$A(k, \omega) = \begin{cases} \sum_e |\langle \psi_e | c_k^\dagger | \psi_0 \rangle|^2 \delta(\omega + \mu + E_0^{(N)} - E_e^{(N+1)}), & \omega > 0 \\ \sum_e |\langle \psi_e | c_k | \psi_0 \rangle|^2 \delta(\omega + \mu - E_0^{(N)} + E_e^{(N-1)}), & \omega < 0 \end{cases} \quad (16)$$

with μ the chemical potential. As shown in Section 2, the photocurrent can then be written:

$$I(k, \omega) = I_0(k, \nu, \vec{A}) A(k, \omega) f(\omega) * R(k, \omega) \quad (17)$$

R being the resolution function of our ARPES experiment, f the Fermi function, and I_0 depending on one-electron matrix elements.

From the Green's function of an interacting system, we can also directly obtain the Fermi surface of the system, as the locus of the k-points where the denominator vanishes for $\omega = 0$:

$$\mu - \epsilon_{k_F} - \Sigma_{m\sigma}(k_F, 0) = 0 \quad (18)$$

Finally, magnetic properties such as susceptibilities, charge-charge or current-current correlation functions can also be calculated, and optical conductivities [44] can be extracted. Thus, we are able to predict much about the behavior of a solid only by knowing its Green's function, and we get not only information about the ground state – as is the case in DFT – but also about excitations, which makes this framework so appealing.

4. Spectral properties of transition-metal pnictides and chalcogenides

4.1. General features of the electronic structure of iron pnictides and chalcogenides

Typical undoped iron pnictides have a nominal band filling of 6 electrons in the Fe-d shell, and one can draw a phase diagram around this filling with – for some materials – a superconducting dome on each side – electron-doped and hole-doped. At this particular filling, realized in most Fe-based pnictides and chalcogenides (such as pure BaFe_2As_2 , LiFeAs , LaFeAsO and FeSe), the Fermi surface is typically formed by three hole pockets and two electron pockets of Fe-d character at the Γ and M points respectively. Figs. 6 and 7 show the DFT-LDA band structure of the prototypical BaFe_2As_2 compound. The iron bands are grouped together around the Fermi level with a total bandwidth of about 4-5 eV, with the Fermi level at

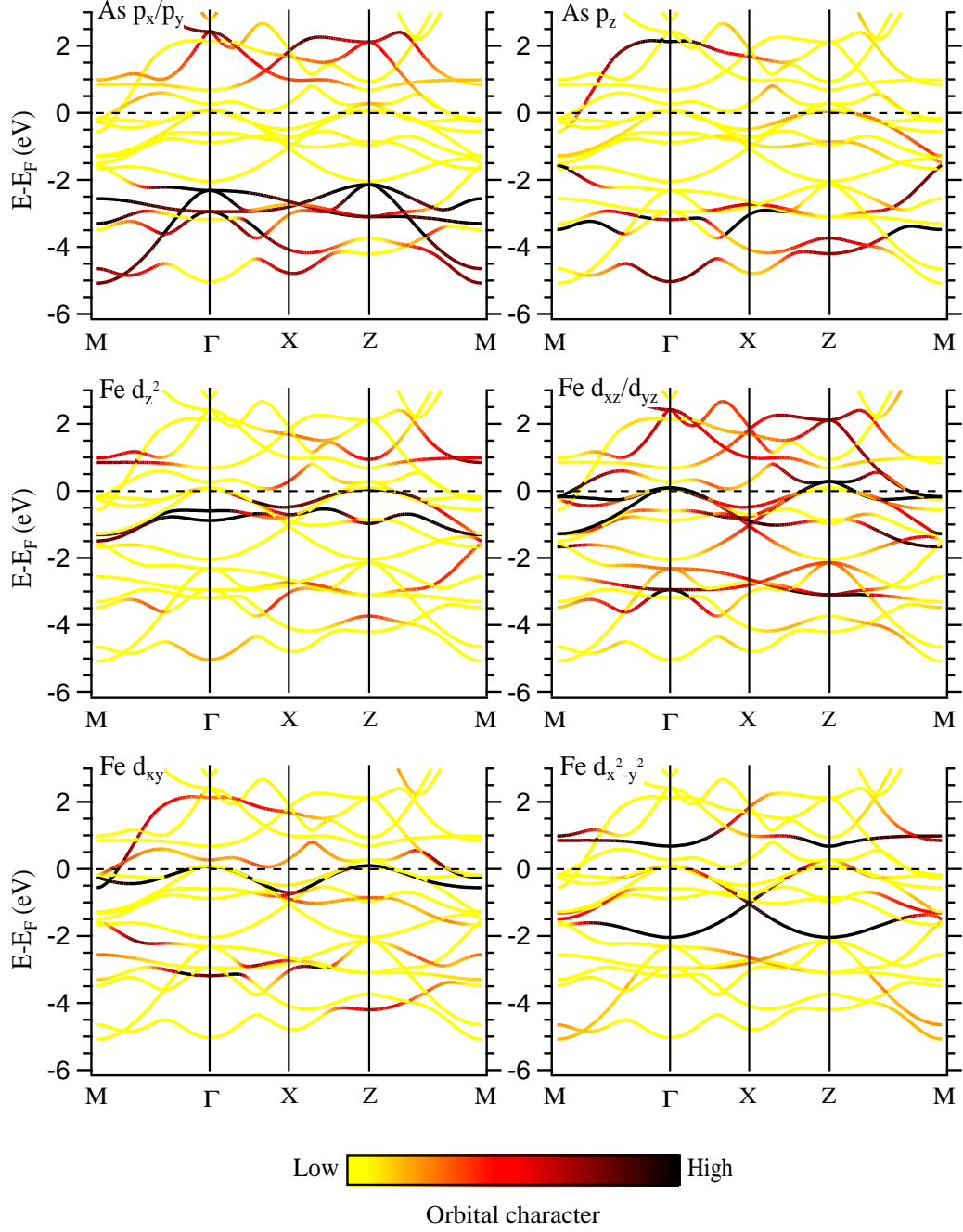


Figure 6: Kohn-Sham band structure of BaFe_2As_2 calculated within the local density approximation (LDA) to DFT. The experimental lattice structure (Ref. [45]) was used in the calculations. The color coding indicates the respective orbital character as given in the upper left corner of each panel.

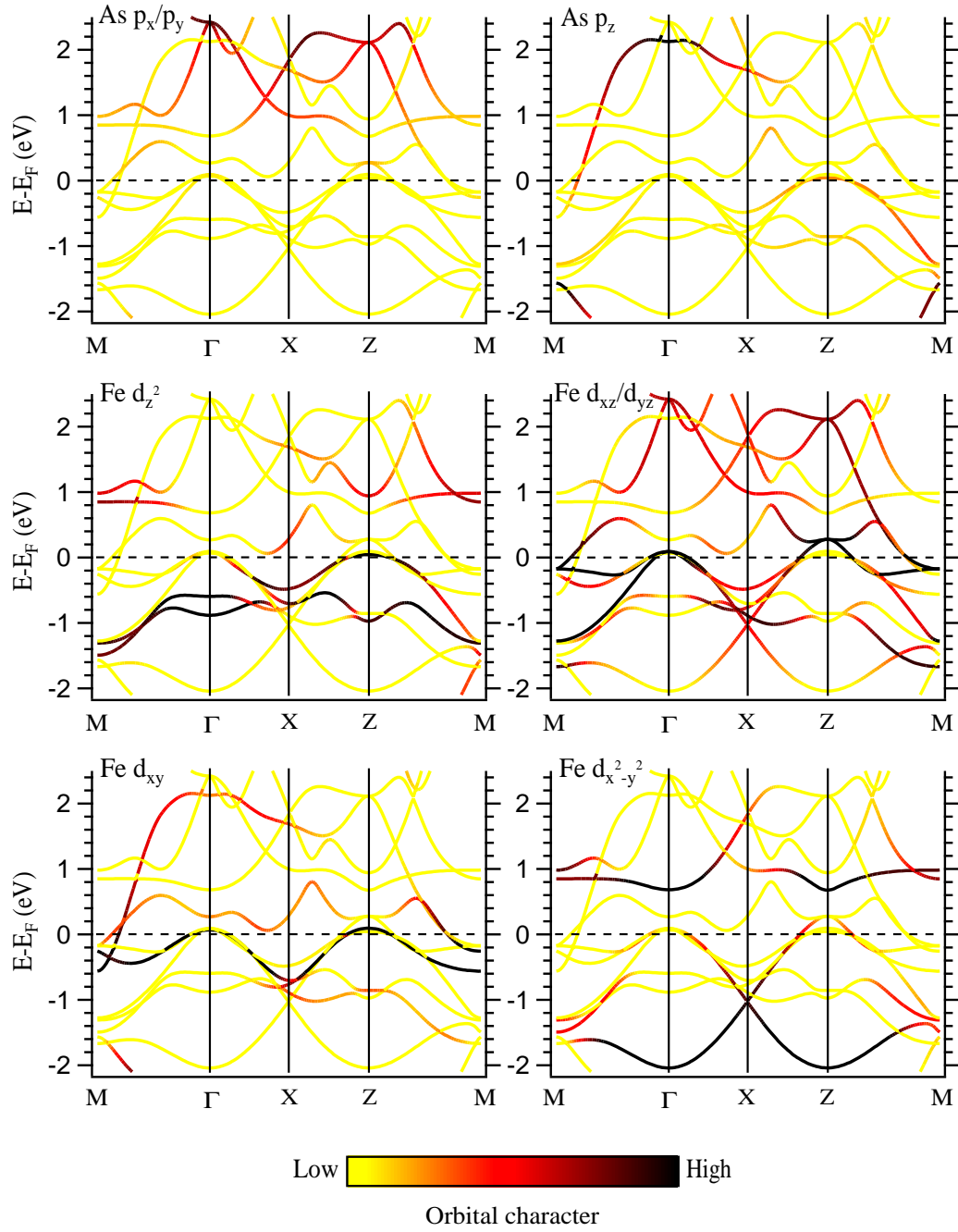


Figure 7: Same as Fig. 6 with a zoom on the Fe- d bands.

filling 6/10. The As- p energy bands lie below the Fe- d bands, approximately between -2 eV and -6 eV. The presence of an energy gap between iron and arsenic bands depends on the compound, but quite generally there is non-negligible hybridization between As and Fe spreading some As-character to the Fe-dominated bands and vice versa. This effect is visible from the color representation in Figs. 6 and 7. One of the most interesting points of the one-particle electronic structure of the iron pnictides is the existence of a “pseudogap” in the density of states of the $d_{x^2-y^2}$ and d_{z^2} orbitals due to the particular structure of the FeAs plane. It implies that the weight of these orbitals is generally small in the low-energy excitations (see Figures 6 and 7). We stress that this is an effect of the single particle band structure, not to be confused with pseudogap behavior induced by many-body correlations.

Substitutions can be performed on every atom of the crystal, which can result in a wide variety of electronic structures. For example, substituting iron with cobalt – 7 electrons in the d shell – generally places the compounds close to a ferromagnetic instability due to a flat band near the Fermi level [46, 47], while increasing even more the number of electrons will push the Fermi level close to a back-bending, “camelback”-shaped energy band [48].

For a detailed analysis of the one-particle band structure of iron pnictides, we recommend the comprehensive work of Andersen and Boeri [18].

4.2. Beyond the single-particle picture: a challenge to theory

Much theoretical work has been carried out to explore the role of electronic correlations beyond the band picture, see e.g. [49, 40, 50, 51, 52, 53, 30, 54] for a by far non-exhaustive list of examples. Important early insights were the discovery of a large dependence of the physics on the Hund’s coupling [55, 56, 50, 30] and the number of d -electrons [57, 30]. We will come back to these points below.

Early on, the strength of the electronic Coulomb correlations has appeared to be an important issue but also a source of controversy [55, 49, 53, 58, 59, 40], emphasizing the subtleties in the construction of the low-energy Hamiltonian and the values of the Hubbard and Hund’s interactions. In fact, the resulting spectra of a DMFT calculation depend crucially on the way the multi-orbital Hubbard-type Hamiltonian is constructed, concerning the energy window chosen for the low-energy description, the construction of the corresponding local orbitals, the interaction terms, and the double counting, see [40] for more details. This sensitivity is largely a consequence of the above mentioned dependence on Hund’s coupling and d -orbital filling since different orbital choices for example lead to different definitions of what one might want to call a d -electron. Most importantly, these difficulties have made iron pnictides and chalcogenides into a crucial playground for benchmarking different strategies.

Substantial efforts in arriving at a truly *ab-initio* description were spent for example in [40], using insights of [60]: The approach developed in that work was based on a Hamiltonian that incorporated both Fe $3d$ and ligand As and O p states as degrees of freedom for LaFeAsO, but with a Coulomb energy cost on Fe $3d$ orbitals only. The many-body Hamiltonian was then solved within LDA+DMFT. The effective interactions for this specific low-energy model were calculated within the constrained random phase approximation (cRPA) [24] – an approach for deriving from first-principles the interacting Hamiltonian within a target subspace that is appropriate for the description of the low-energy many-body properties. Within this scheme, LaFeAsO was described as a metal with moderate strength of the electronic correlations [40], whereas larger effects were found for α -FeSe [50].

4.3. ARPES on iron pnictides and chalcogenides – General remarks

In the whole pnictide family, photoemission measurements are able to identify band dispersions and a Fermi surface.

A difficulty stems from the surface sensitivity of ARPES, though. Indeed, ARPES usually probes the surface in the photon energy considered, and the measured energies can be quite different from the bulk band structure. Surface effects were predicted in LaFeAsO in Ref. [61], due to the polar character of the surface. The most important surface effects seem to appear in the 1111 family, due to the polar cleavage surface that creates an important modification of the potential [5, 62, 63]. Two main effects can appear and can depend on which plane forms the surface: the appearance of additional bands, which have been

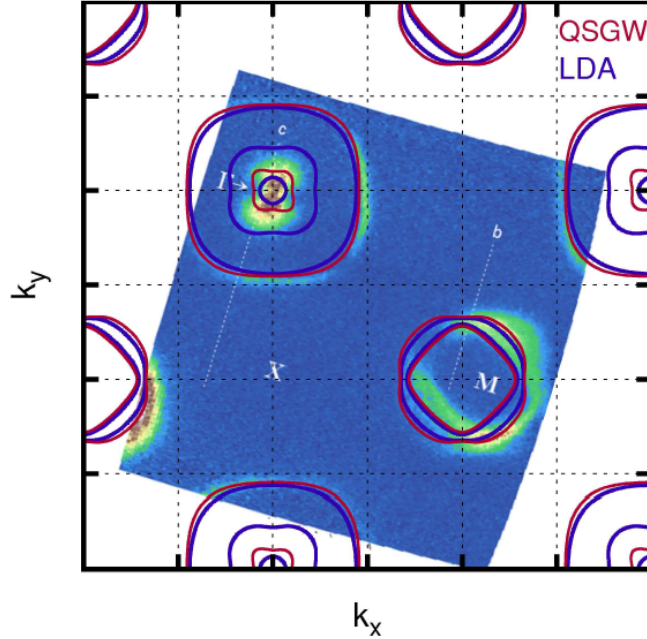


Figure 8: Fermi surface of LiFeAs from QSGW and LDA compared to the experimental ARPES spectrum from [71]. $k_z = 0$ plane in the Brillouin zone for 2 Fe atoms. One of the hole pockets at Γ sinks below the Fermi level in GW, and another shrinks drastically, in agreement with photoemission. (Reprinted with permission from Ref. [72], copyright ©(2012) by The American Physical Society.)

probed for instance in LaFeAsO [62] or SrFe₂As₂ [64], or the modification of the total electron count such as in LaFePO [65]. Surface effects have also been identified in BaFe_{2-x}Co_xAs₂ [66], as well as in BaCu₂As₂ [67], where a simple structural model suggests a relaxation of the As-position to be the main effect. In the following, to keep the discussion simple we will focus on materials without or with limited surface effects.

At first glance, band structures calculated from density functional theory in the local density approximation (LDA) roughly correspond to the measured quasiparticles, except that they have to be renormalized by a factor of about 2 to 5 depending on the material [5, 68]. This confirms that the iron pnictides are indeed metals constituted of itinerant quasiparticles with an enhanced effective mass produced by intermediate correlations.¹ Correlation effects are stronger when moving to the iron chalcogenides: Indeed, in FeSe, a Hubbard band has been predicted [50] and observed [70, 68].

4.4. Fermi surfaces: theory vs. experiment

The determination of the Fermi surfaces and low-energy excitations of transition metal pnictides is believed to be a key issue for the understanding of the phase diagram and mechanism for superconductivity. ARPES has been used to systematically map out quasi-particle dispersions, and to identify electron and hole pockets potentially relevant for low-energy instabilities [73, 74, 75, 76, 77, 78, 79]. Density functional theory (DFT) calculations have complemented the picture, yielding information about orbital characters [80], or the dependence of the topology of the Fermi surface on structural parameters or element substitution [81, 82].

The overall picture emerging from these studies is that for many pnictides the general topology of the Fermi surface measured within ARPES coincides with the one obtained from DFT, although quantitative differences in the pocket sizes (with, most of the time, smaller pockets in nature than in theory) are common.

¹It is worth noting that the binding energy of itinerant As-4*p* states is also underestimated by the LDA [69, 65], though for slightly different reasons: this is the analog of the usual “band gap” problem of DFT-LDA.

On those, there seems to emerge some agreement that combined DFT+DMFT calculations yield corrections in the right direction, though not always of large enough size. Limitations have been pointed out, e.g. in $\text{Ba(Fe,Co)}_2\text{As}_2$, where ARPES has evidenced persisting discrepancies in comparison with both DFT and DFT+DMFT calculations [83]. In BaFe_2As_2 , the d_{xy} band is found to form a third hole pocket in the calculations while a maximum around -150 meV below the Fermi level is captured by photoemission [84, 85]². A similar discrepancy was also revealed in hole-doped $\text{Ba}_{0.6}\text{K}_{0.4}\text{Fe}_2\text{As}_2$, where the band-top of the inner hole pocket, detected from high-temperature measurements, was found lower than in LDA calculations [89].

Even more serious problems arise in FeSe: The LDA Fermi surface takes the standard form of three hole pockets (of which two appear to be quasi-degenerate) and two electron pockets. While including correlations substantially improves on the general band dispersions [50] and somewhat reduces the size of the pockets, no drastic changes to the Fermi surface result. Experimentally, the literature documents a continuous struggle for determining the number, size and k_z -dispersion of the pockets [90, 91, 92, 93, 94, 95, 96, 97, 98, 99], and the situation is still not fully clear. Still, there seems to emerge some consensus on *tiny* energy scales of the pocket depths (measured in meVs and thus of the order of the gap) raising speculations about highly unconventional types of superconductivity. Furthermore, rather unconventional behaviors have been observed when cooling FeSe into its low-temperature orthorhombic phase, where spin-orbit coupling and possible orbital order are invoked to rationalize the observed degeneracies and absence thereof. To the best of our knowledge, no *ab initio* method has so far been able to describe these properties. For a discussion of the construction of an effective tight-binding model parameterizing the correlated electronic band structure, see the Review by P. Hirschfeld in this volume.

Finally, another particularly interesting example is LiFeAs where DFT-LDA underestimates the size of the outer hole pocket at the Γ point, compensated by a gross overestimation of the size of the inner ones. Experimentally it was difficult to reach agreement even on the number of pockets since a band just touching the Fermi level is sometimes but not always resolved as forming a Fermi surface [100, 101, 102, 71].

Interestingly, many-body perturbation theory approximating the self-energy by its first order term in the screened Coulomb interaction W (so-called “GW approximation”) results in a substantially improved description: quasi-particle self-consistent (QS)GW [103] calculations found momentum-dependent corrections to the LDA Fermi surfaces to result in a suppression of the innermost pocket [72]. The Fermi surface within QSGW thus shows only two hole pockets around the center of the Brillouin zone [72] compared to three in LDA or LDA+DMFT [104, 51, 88] with the overall size in better agreement with photoemission measurements than the LDA Fermi surface (see Figure 8). These observations indicate that combined schemes retaining the advantages of the GW approximation such as the calculation of non-local exchange and of the non-perturbative computation of correlation effects from DMFT is a promising way. A similar correction to the Fermi surface due to non-local exchange was indeed found in the cobalt compound BaCo_2As_2 [47]. We come back to this point in the section on recent theoretical developments.

It was argued that the effect of spin-orbit coupling is primordial for the description of the Fermi surface, since it can lift some degeneracies very close to the Fermi level in the d_{xz}/d_{yz} orbital space, notably for the hole pockets at the Γ point and for the electron pockets along the MX direction [105]. The compounds in which such effects have been discussed are again FeSe and LiFeAs. Indeed, in LiFeAs two of the usual hole pockets at the Γ point can be distinguished by ARPES, while if the spin-orbit coupling could be neglected these bands should be degenerate. In this context, Borisenko and collaborators attempted to extract an estimate for the spin-orbit coupling strength, arriving at a value of around 10 meV [105] (see Figure 9). Nevertheless, some mysteries also remain which might contradict the interpretation as a pure spin-orbit effect: i) the splitting is temperature dependent; ii) the splitting is strongly doping-dependent; iii) There is not so much difference between As, Se and Te. Together with the quite universally observed

²It is interesting to note that if the arsenic height is moved away from the experimental crystal structure in order to minimize the LDA energy, the position of the d_{xy} band at the Γ point can be dramatically modified [81, 80, 86]. In some cases, the band structure then found can be closer to the ARPES measurements, albeit for the wrong reason. In particular, in BaFe_2As_2 the maximum around -150 meV captured by photoemission is reproduced [84]. Within DFT+DMFT, the optimized arsenic height is much closer to the experimental structure [87, 88].

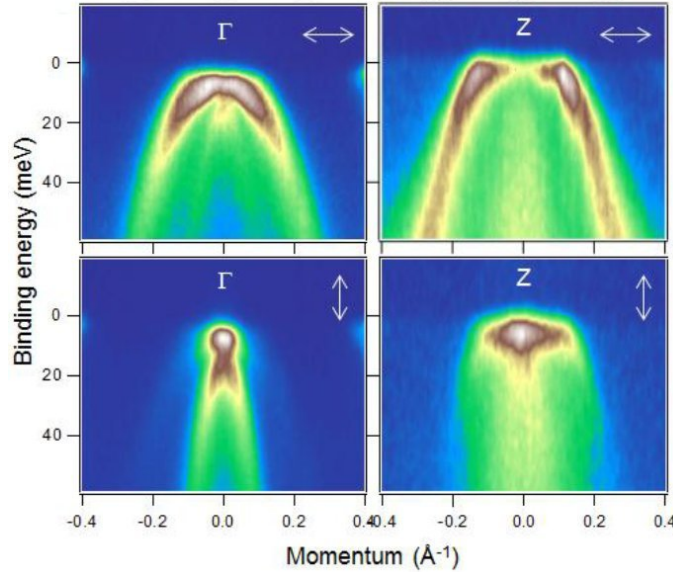


Figure 9: High-resolution low-temperature ARPES data near Γ and Z points recorded with the light of horizontal (upper) and vertical (lower) polarizations in LiFeAs. The degeneracy of the two bands at zero momentum is lifted, possibly by spin-orbit coupling. Reprinted with permission from Ref. [105].

indications hinting at an influence of nematic fluctuations in the proximity to structural phase transitions, one might speculate that the final picture might be a cooperative interplay of different ingredients. These issues clearly deserve further investigations.

4.5. Bandwidth trends and comparison to electronic structure calculations

Assessing the strength of the band structure renormalization allows us to extract general tendencies concerning the strength of electronic correlations. Within a same family, and if the crystal structure is not modified by the introduction of impurities, hole-doping increases the band renormalization while electron-doping reduces it. This goes hand in hand with a trend in coherence properties predicted from first principles calculations [30]: while the electron-doped Ba122 compound is in a Fermi liquid regime, the coherence properties degrade when moving to the hole-doped side, where Hund’s coupling induces a “fractional self-energy” regime at intermediate temperatures, thus considerably suppressing the coherence temperature where true Fermi liquid behavior sets in. We will come back to this point below.

The trend on quasi-particle renormalization is most easily seen in the BaFe_2As_2 family in the paramagnetic state: within the same study [106] a factor of 2.7 was found for the hole-doped $\text{Ba}_{0.6}\text{K}_{0.4}\text{Fe}_2\text{As}_2$, of 1.5 for the undoped BaFe_2As_2 and of 1.4 for the electron-doped $\text{BaFe}_{0.88}\text{Co}_{0.12}\text{As}_2$. The 11 family displays the highest renormalization, with factors found in the literature larger than 3.5 [68, 70, 107]. The 111 are an intermediate case with a renormalization factor of 3 – 4 in LiFeAs and NaFeAs [71, 108, 109]. Finally, substituting Fe by Ru in BaFe_2As_2 substantially reduces these effects, due to the less localized 4d shell [110, 111].

Nevertheless, a caveat is in order: Some iron pnictides have been studied extensively by several groups, such as the BaFe_2As_2 family [78, 125, 126, 89, 75, 85, 84, 112, 46, 127, 128], but the magnitude of the renormalization factors found by different ARPES groups shows an impressive discrepancy. Figure 10 shows the diversity of renormalization factors obtained by fitting ARPES data to DFT calculations that can be found in the available literature. If we compare again with the numbers found by Yi and collaborators [106], for electron-doped $\text{BaFe}_{0.84}\text{Co}_{0.16}\text{As}_2$ Brouet and collaborators [117] found a much higher value of 3.3, while for $\text{Ba}_{0.6}\text{K}_{0.4}\text{Fe}_2\text{As}_2$ Ding and collaborators [89] found a lower overall factor of 2. Many ARPES authors have signaled additional momentum-dependent or orbital-dependent shifts of the band structure

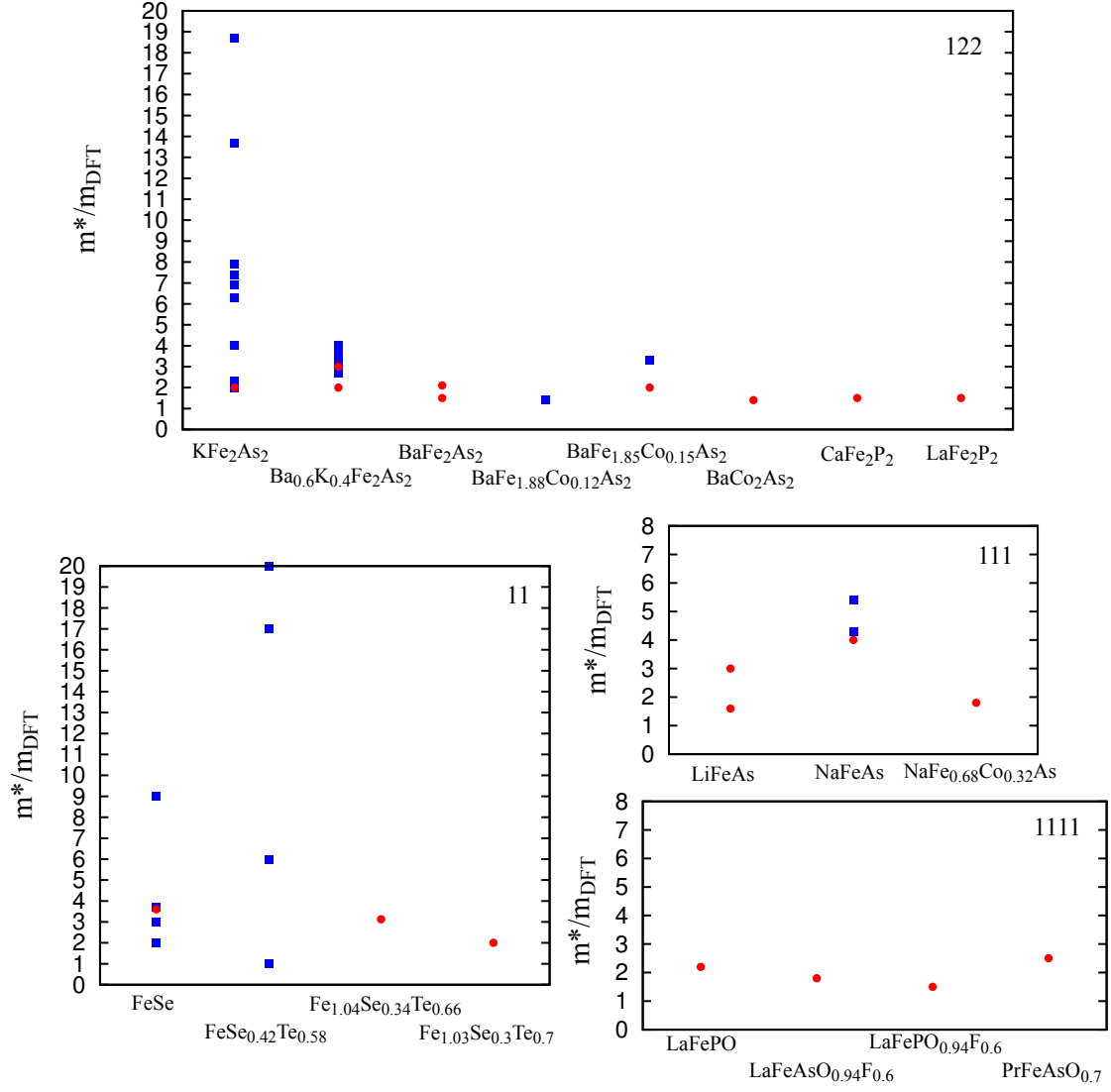


Figure 10: Effective mass obtained from ARPES experiments compared to DFT calculations in different families of iron pnictides. Red dots correspond to an overall renormalization factor obtained for all bands on an extended energy range, while blue squares correspond to low-energy, orbital-dependent or momentum-dependent renormalization factors. Data was taken from Refs. [112, 113, 89, 106, 114, 115, 116, 117, 46] for the 122, Refs. [68, 91, 107, 118, 119] for the 11, Refs. [71, 120, 108, 121, 122] for the 111 and Refs. [69, 123, 124] for the 1111.

[106, 110, 89, 71, 78] or orbital-dependent renormalizations [69, 89, 112, 129, 83, 107, 126]. The orbital-dependence of renormalization is clearly captured by DMFT, and it has even been proposed that iron pnictides are in the proximity of an orbital-selective Mott transition [130, 56, 131, 31] (see Section 4.7). On the other hand, it is interesting to note that at the GW level, the orbital renormalizations have been found to be independent of the momentum at low energy, while momentum-dependent corrections to DFT bands are due to non-local exchange and correlations [72].

4.6. Hund’s coupling and “spin-freezing” regime

Hund’s rule coupling J_H plays a fundamental role for the physics of iron pnictides. Early on, in [55], a coherence-incoherence crossover in the electronic properties of LaFeAsO was identified, and the exploration of the – sometimes counterintuitive – consequences of Hund’s exchange continues to be an active topic in the field. In this section, we give some background on how to put different observations related to this physics into perspective.

As discussed in the preceding sections, band structures calculated from DFT provide a useful starting point for the description of spectral properties of iron pnictides, in the sense that most often the overall picture in terms of Fermi surface topology and quasi-particle dispersions can be matched (even though, of course, for a quantitative description shifts or renormalizations may be required). These findings document the validity of the Landau Fermi liquid picture for these compounds. Still, the energy scales below which the quasi-particle picture is well-defined can largely vary – from compound to compound, under doping or pressure, and even from orbital to orbital in a given material.

Before coming back to this point, let us note that it is an easy task to enumerate a whole list of experimental observations that document effects lying outside the coherent Fermi liquid regime: (a) Ding and collaborators [89] noted energy-dependent renormalizations of the band structure, with an enhanced factor near the Fermi level. This means that the electronic structure of such compounds cannot be interpreted in a Fermi-liquid picture with a renormalization factor Z , at least at the temperature of the measurement. (b) Recently, the existence of a coherence-incoherence crossover as a function of the isovalent Te-Se substitution has been investigated in Ref. [132] (see Figure 11). The authors found much shorter quasiparticle lifetimes in fully substituted FeTe and postulated a relationship to the development of antiferromagnetism. (c) Finally, temperature-dependent measurements reveal other surprising effects: Brouet and collaborators [83] found an evolution of the number of carriers via k -dependent shifts on the Fermi surface, while (d) Yi and collaborators [129] investigated an orbital-selective coherence-incoherence crossover in alkali-intercalated iron selenide. This list could be continued nearly *ad libitum*. We also refer the reader to the detailed review by Florence Rullier-Albenque in this volume, which deals with transport properties of iron pnictides, documenting various badly metallic regimes.

On the theoretical side, we highlight a theoretical study that was performed independently of the discovery of superconductivity in the iron pnictides: a DMFT study of a three-band orbital Hubbard model with a local interaction parameterized by Hubbard interactions and Hund’s exchange at filling $2/6$ or $4/6$ [136] revealed the existence of a “spin-freezing” regime characterized by a power-law behavior of the imaginary part of the self-energy in Matsubara frequencies, corresponding to an incoherent metal. This regime is characterized by strong Hund’s coupling favoring a high-spin state strongly suppressing charge fluctuations. Kondo screening of the effective impurity in the DMFT description – which, in the DMFT language, is a necessary condition for the formation of a coherent Fermi liquid state – is thus suppressed and Fermi liquid behavior is recovered only below a possibly extremely low coherence temperature. Most interestingly, in [30], such a power-law regime of the self-energy was later on detected in calculations for iron pnictides, namely for hole-doped BaFe_2As_2 (see Figure 12). While in a three-orbital model, the spin-freezing regime is realized around fillings $2/3$ or $4/6$, that is, around even commensurate fillings, the analogous situation in a 5-orbital system includes precisely the $6/10$ filling of the nominal valence of the iron pnictides. In [30], the phase diagram around this filling – corresponding to pure, hole- or electron-doped BaFe_2As_2 was found to display the same phenomenology as in the three-orbital model: Fermi liquid behavior was enhanced (that is, the coherence temperature increased) under electron doping, moving the system further away from the half-filled $5/10$ case, while the incoherent “spin-freezing” regime was evidenced as the intermediate temperature regime under hole-doping, that is, for fillings $(6-x)/10$. The exploration of the consequences of Hund’s coupling in

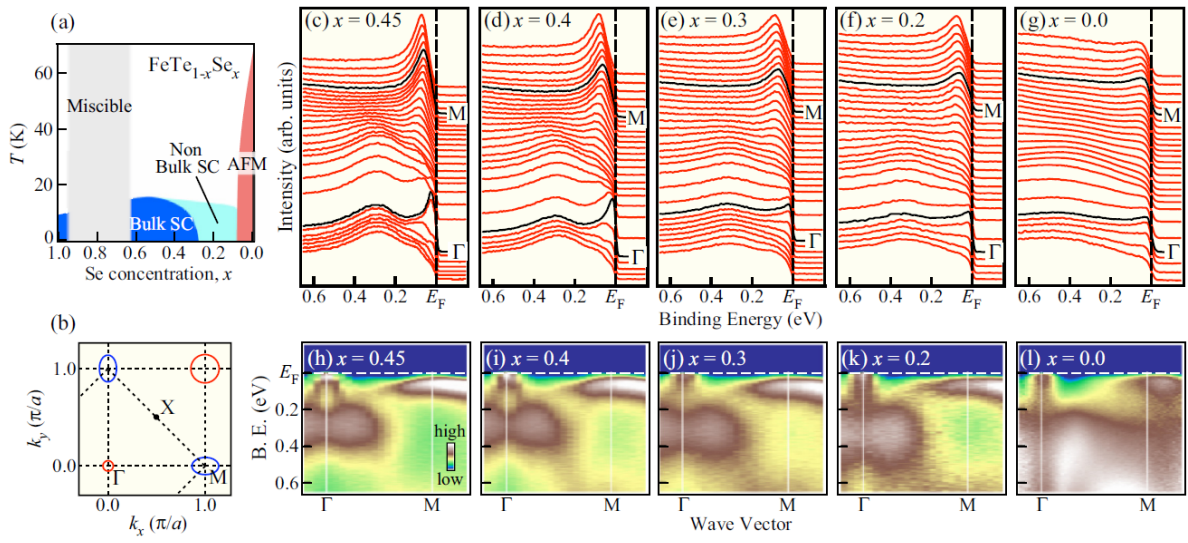


Figure 11: Coherence-incoherence crossover in $\text{FeTe}_{1-x}\text{Se}_x$ (reprinted with permission from Ref. [132], copyright ©(2014) by The American Physical Society):

(a) Schematic phase diagram of $\text{FeTe}_{1-x}\text{Se}_x$ derived from Ref. [133, 134, 135]. SC and AFM denote superconductivity and antiferromagnetism, respectively. The miscible region exists at high Se concentrations due to the difficulty in growing single-phase samples.

(b) One-Fe/unit-cell Brillouin zone of $\text{FeTe}_{1-x}\text{Se}_x$ together with the schematic hole and electron Fermi surfaces at the Γ and M points, respectively.

(c)–(g) Se-concentration dependence of normal-state ARPES spectra along the Γ -M line in a wide energy region for $\text{FeTe}_{1-x}\text{Se}_x$ ($T = 25$ K for $x = 0.45-0.2$ and 80 K for $x = 0.0$) measured with the He-I α resonance line ($\hbar\nu = 21.218$ eV).

(h)–(l) Corresponding ARPES intensity plotted as a function of binding energy and wave vector.

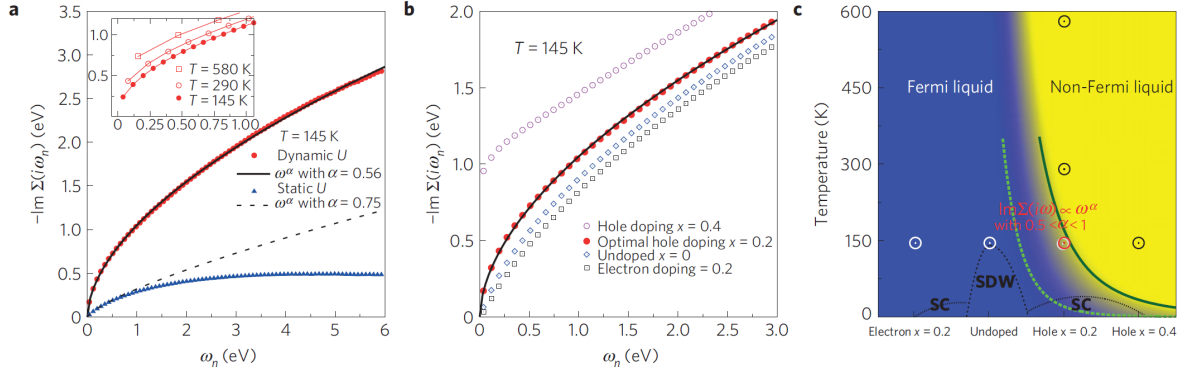


Figure 12: Fractional power-law behavior of the self-energy in $\text{Ba}_{1-x}\text{K}_x\text{Fe}_2\text{As}_2$ (reprinted with permission from Ref. [30]). (a) Imaginary part of the self-energy (orbital average) on the Matsubara axis for optimal hole-doping ($x=0.2$ per Fe) within LDA+DMFT, with dynamical interaction $U(\omega)$ (red circles) and static $U(\omega = 0)$ (blue triangles). Solid and dashed lines are fits of the low-frequency behavior of the function $-\text{Im}\Sigma(i\omega_n) = A(\omega_n)^\alpha$. The inset shows the low-frequency behavior of the dynamic- U result for different temperatures. As the temperature is raised, the extrapolation $\omega_n \rightarrow 0$ yields a non-zero intercept, which indicates that even excitations at the Fermi level exhibit a finite lifetime. (b) Low-energy behavior of the self-energy as a function of doping. Fermi-liquid behavior is found in the undoped and electron-doped compounds, whereas a non-zero intercept appears in the overdoped case. (c) Sketch of the phase diagram in the space of temperature and doping. The blue region indicates Fermi-liquid behavior, whereas yellow indicates a frequency dependence of the self-energy that is not compatible with Fermi-liquid theory. The light green dashed line marks the boundary of the crossover region, where the exponent α starts to deviate from 1. The dark green solid line corresponds to $\alpha = 0.5$, which marks the “spin-freezing” transition. To the right of this line, an incoherent metal phase with a non-zero intercept of $\text{Im}\Sigma$ is found. The experimentally measured phase diagram with superconducting (SC) and spin-density wave (SDW) ordered phases is indicated by black dotted lines. Full substitution (KFe_2As_2) corresponds to $x=0.5$.

iron pnictides has therefore become an active area of research, including the limits of the local description of DMFT [137] or analytical insights from a renormalization group treatment [138]. As discussed on the basis of zero-temperature calculations [31], at low-temperatures (that is, within the coherent regime) the filling dependence of the Fermi liquid properties translates into an evolution from a more strongly correlated state (characterized by a small quasi-particle weight Z) close to half-filling to a less correlated state at fillings $6+x$.

Model studies have pushed this picture further by analyzing the orbital dependence of the renormalization factors: De’ Medici and collaborators have argued that the strong Hund’s coupling can decouple the Fe- d orbitals and drive them close to a Mott-selective phase [31, 130, 56, 131] where the d_{xy} orbital would be the most strongly correlated orbital. While this general trend agrees well with results from more realistic DMFT calculations (in particular, concerning the less correlated z^2 and $x^2 - y^2$ orbitals, due to their one-particle pseudogap [50]), the quantitative aspects of this differentiation seem to be considerably stronger in the model context where only the five d -orbitals are retained, than in electronic structure calculations where also pnictogen/chalcogen p -states are included.

4.7. Weak coupling or strong coupling? – Are iron pnictides siblings of cuprates?

As we have seen, in the pnictides and chalcogenides the variety of compounds and fillings of the d shell combined to the great sensitivity of correlations due to the large Hund’s coupling account for a wide diversity of behaviors. In this section, we will focus on the more strongly correlated features and on the possible similarities with the cuprates. As alluded to at several points in this review already, the most correlated family are the chalcogenides, notably due to the smaller hybridization between Fe and Se. In FeSe, the existence of a broad feature of Fe- d character around -2 eV in the photoemission spectrum has been revealed in Ref. [70, 68] and was identified as a Hubbard band by Aichhorn and collaborators [50]. The stronger correlations in FeSe also come along with a more pronounced orbital differentiation, namely more strongly correlated xy - and xz/yz -orbitals. This is quite natural due to the (single-particle-) pseudogap of the z^2 and $x^2 - y^2$ orbitals at the Fermi level [50].

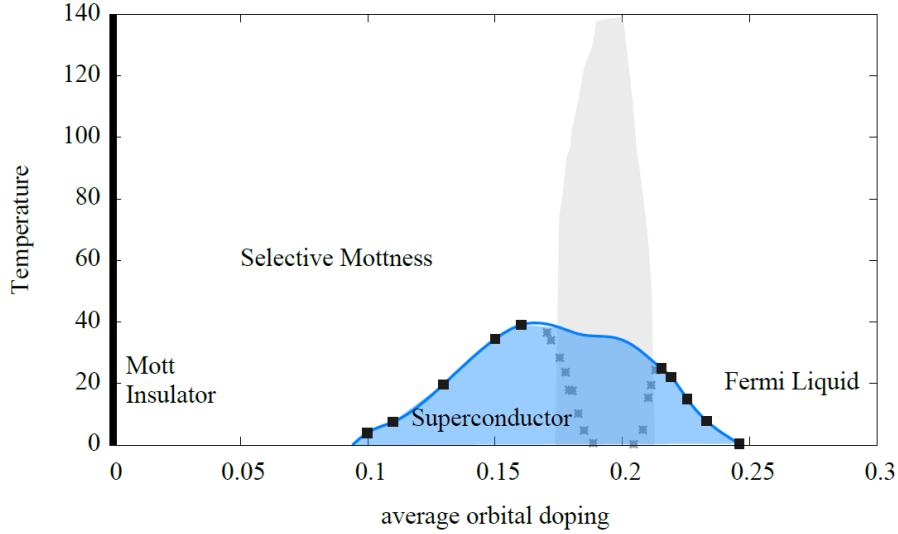


Figure 13: Possible unified phase diagram for pnictides and cuprates reprinted with permission from Ref. [31], copyright ©(2014) by The American Physical Society. Plotted here is the experimental phase diagram for doped BaFe_2As_2 as a function of the average orbital doping. In the hypothesis that the magnetically ordered/orthorhombically distorted phase (grey area) is accidentally favored by the total commensurate filling $n=6$ around the stoichiometric compound thus suppressing the superconductivity of the tetragonal phase, de' Medici and collaborators artificially eliminate it and complete the superconducting dome (blue area).

In $\text{Fe}_{1.06}\text{Te}$, photoemission found a pseudogap in the paramagnetic phase, progressively closing when the temperature is reduced in the antiferromagnetic phase [139]. Interestingly, a pseudogap was also measured in underdoped $\text{Ba}_{1-x}\text{K}_x\text{Fe}_2\text{As}_2$ [140], and the relation between those two experiments remains to be understood. More experimental evidence would be desirable to confirm the existence of a pseudogap in iron pnictides and probe its characteristics.

Finally, we mention that in the quest of similarities with the cuprates, several authors have argued in favor of an analogy of the phase diagrams when the average filling per orbital is considered [31, 130, 56, 131, 141]. In this picture, the behavior at filling d^6 is considered as a (magnetic) accident artificially separating the electron- and hole-doped superconducting regions in the phase diagram, and the proximity to the Mott insulator (at filling d^5) would be the key feature linking cuprate and pnictide physics. The corresponding tentative phase diagram is shown in Figure 13.

4.8. Spectral properties in a nutshell

Summarizing, at present, there is a large consensus on the fact that iron pnictides display intermediate correlations – stronger in the 11 family and chalcogenides [50], weaker in the 1111 and phosphides in general – driven by the physics of strong Hund's coupling in multiorbital systems [142, 136]. The consequence is that these materials tend to display a bad-metal behavior, in which the effective mass and the coherence properties are very sensitive to the effective number of electrons in the correlated shell [30, 46], which can be tuned by small details of the electronic structure, notably the hybridization between the metal and the pnictogen [54, 143].

5. Superconducting gap

The previous section raised an important question that is relevant not only to the electronic band structure itself, but to the pairing mechanism as well: weak or strong coupling? To discuss this question, we discuss the order parameter of the superconducting transition, which consists in a complex function of the

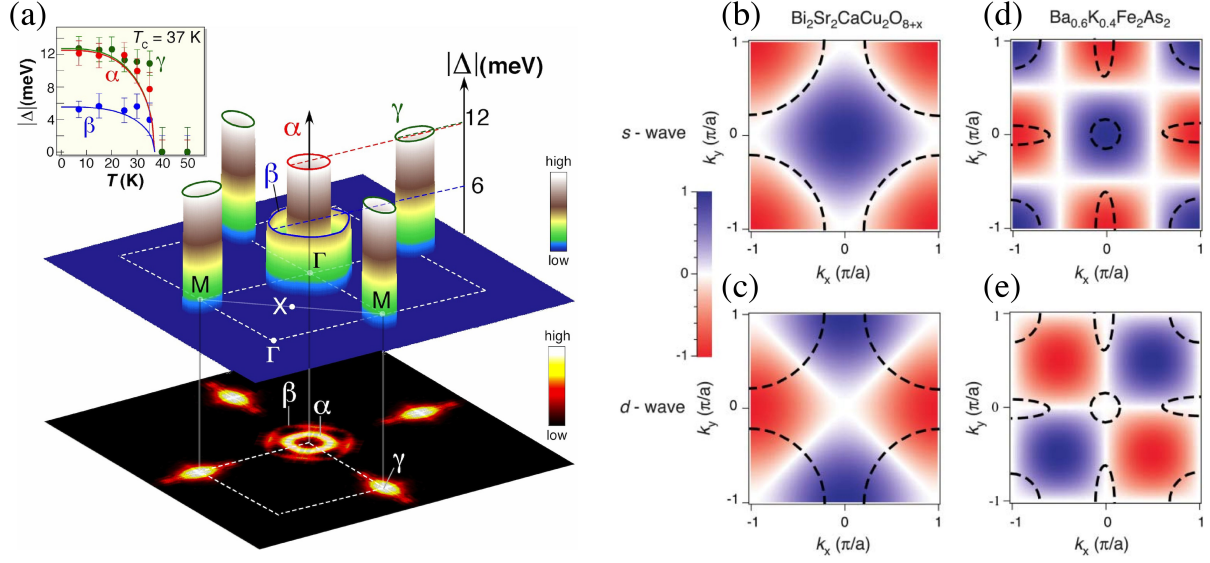


Figure 14: (a) Three-dimensional plot of the SC gap size (Δ) in $\text{Ba}_{0.6}\text{K}_{0.4}\text{Fe}_2\text{As}_2$ measured at 15 K on three Fermi surface sheets (shown at the bottom as an intensity plot) and their temperature evolutions (inset). Reprinted with permission from [144], copyright © (2008) by the European Physical Society. (b)-(e) Visualization of the overlap between Fermi surfaces and gap functions: (b) s -wave $\cos(k_x) + \cos(k_y)$ for optimally doped cuprate $\text{Bi}_2\text{Sr}_2\text{CaCu}_2\text{O}_{8+x}$; (c) d -wave $\cos(k_x) - \cos(k_y)$ for $\text{Bi}_2\text{Sr}_2\text{CaCu}_2\text{O}_{8+x}$. (d) s -wave $\cos(k_x)\cos(k_y)$ for optimally doped ferropnictide $\text{Ba}_{0.6}\text{K}_{0.4}\text{Fe}_2\text{As}_2$. (e) d -wave $\sin(k_x)\sin(k_y)$ for $\text{Ba}_{0.6}\text{K}_{0.4}\text{Fe}_2\text{As}_2$. The color bar indicates the values of the SC order parameters. Panels (b)-(e) are reprinted by permission from Macmillan Publishers Ltd: Sci. Rep. [163], copyright © (2012).

momentum whose amplitude corresponds to the size of an electronic band gap 2Δ developing symmetrically with respect to the Fermi level while cooling down a sample below its superconducting transition temperature. This amplitude Δ is accessible by ARPES directly in the momentum space [144, 145, 146, 119, 71, 147]). The Fermi surface of the first Fe-based superconductors studied [144, 145] contributed to popularize a simple pairing mechanism called quasi-nesting [148, 149, 150, 151, 4]. Indeed, as shown in the bottom part of Fig. 14(a) and discussed the previous section, the Fermi surface is formed by hole pockets centered at Γ and electron pockets centered at M. Within the quasi-nesting model, the pairing amplitude is largely enhanced by electron-hole inter-pocket scattering with the antiferromagnetic wave vector, which coincides with the wave vector from Γ to M. Accordingly, the top of Fig. 14(a) indicates that a large gap is observed on every Fermi surface pockets except the β band, which is much larger than the others and thus not well quasi-nested with any other band. For this mechanism to be effective, it is necessary that the pockets have similar sizes and shapes, but not equal since this would favor a density-wave ground state [152]. Therefore, this weak coupling mechanism is by nature very sensitive to the Fermi surface topology.

There is now some evidence against the weak coupling approach as driving force of the pairing of electrons in the Fe-based superconductors [4]. Perhaps the most significant one is the existence, for the same 122 crystal structure, of at least three distinct Fermi surface topologies leading to superconductivity, which is the equivalent of three fundamentally different sets of critical parameters, a possibility not appealing physically. Indeed, $\text{Ba}_{1-x}\text{K}_x\text{Fe}_2\text{As}_2$ has the Fermi surface topology displayed in Fig. 14(a) and refined later [153]. With approximately the same critical temperature as $\text{Ba}_{1-x}\text{K}_x\text{Fe}_2\text{As}_2$, the 122-ferrochalcogenides $\text{A}_x\text{Fe}_{2-x}\text{Se}_2$ [154, 155] have a drastically different Fermi surface topology with no hole pocket [156, 157, 158, 159, 160]. Finally, due to a chemical potential shift resulting from hole-doping, the electron pockets at M are replaced by four petal-shaped lobes in KFe_2As_2 , which are off-M centered [161, 162].

In contrast to the weak coupling approach, a strong coupling approach to the pairing is much more robust to the evolution of the Fermi surface. This is the case of the $J_1 - J_2 - J_3$ model, where J_1 , J_2 and J_3 represent the exchange parameters between first, second and third nearest neighbor, respectively. The

philosophy of this approach is to parameterize the magnetic structure of a parent compound by effective coupling parameters J_i . We note that – as shown first by Yaresko et al. [164] – a more appropriate parameterization is provided by assuming biquadratic exchange terms. For the sake of simplicity, we stick here to the simpler $J_1 - J_2 - J_3$ model, but refer the reader to the detailed discussion of the biquadratic model in the Review by P. Hirschfeld in this volume. In momentum space, the structure of the interactions determines a form factor consisting of combinations of sine and cosine functions. If the pairing is induced by the fluctuations of the local moments away from long-range magnetic ordering, the pairing symmetry can be assumed to have the same form factor. However, a few possibilities exist due to the relative phase of the different interactions. Given the fact that the energy of the whole system should be lowered by gapping electronic states near the Fermi level, one can assume the favored symmetry to be the one which maximizes the overlap between the Fermi surface and the antiferromagnetic form factor [163, 4]. We first illustrate this with the cuprates. These materials are well known for having a dominant J_1 antiferromagnetic exchange parameter which leads to a possible s -wave gap function and a possible d -wave gap function, as shown in Figs. 14(b) and 14(c), respectively. Despite nodes, the overlap with the d -wave gap function is much better. In contrast, the dominant antiferromagnetic exchange parameter in the Fe-ferropnictides is J_2 , which also leads to different s -wave and d -wave gap functions (see Figs. 14(d) and 14(e)), and in that case the overlap of the Fermi surface is better with the s -wave (the so-called s_{\pm} gap function), with the same gap amplitude for the Γ -centered hole pockets and M-centered electron pocket that have the same size, as observed experimentally. Interestingly, in the ferrochalcogenides neutron data indicate a non-negligible J_3 in addition to J_2 , which induces an asymmetry of the gap function between the Γ and M points. Such an asymmetry would be consistent with what has been found experimentally for $\text{FeTe}_{0.55}\text{Se}_{0.45}$ [165].

Still, we stress again the simplistic nature of these fully localized models, let it be the $J_1 - J_2 - J_3$ model or its biquadratic refinements. On conceptual grounds it is difficult to justify a purely strong coupling approach. In practice, a much debated case is LiFeAs , where a measured noticeable anisotropy in the superconducting gap around the M point [100, 101] has been interpreted as evidence for effects beyond the localized picture. An alternative scenario, dubbed orbital anti-phase s_{\pm} gap function, has been proposed on theoretical grounds [166, 167]. This is a variant of the s_{\pm} scenario, where the phase of the superconducting gap depends on the orbital character. The observation by ARPES of an in-gap impurity states in $\text{Ba}_{1-x}\text{K}_x\text{Fe}_2\text{As}_2$ was argued to be consistent with this hypothesis [168].

6. Recent theoretical developments

A topic that has raised much interest recently is the *ab initio* determination of the Hubbard interactions, including their dynamical character and the consequences thereof. The impact of the energy-dependence of the Hubbard interactions – $U(\omega)$ as calculated within constrained-RPA – on the low-energy properties and the coupling between electronic and plasmonic excitations in the many-body calculations, has been investigated in prototypical models [169] and then applied to BaFe_2As_2 [30] in a study revealing the spin-freezing phase in the hole-doped side of the phase diagram (see Figure 12). The inclusion of energy-dependent Hubbard interactions within a dynamical version of LDA+DMFT [169, 30], leads to a reduction of the quasi-particle weight at the Fermi energy, compared to the standard LDA+DMFT with a static interaction. The spectral weight is shifted to additional satellites at larger energies corresponding to plasmon excitations. This transfer of spectral weight is accompanied by a corresponding reduction of the bandwidth, and can be understood as an effective renormalization of the one-particle hopping matrix elements by the dynamical screening processes. The quantitative aspects of this effect depend on the spectrum of (bosonic) screening processes as encoded in the frequency-dependence of $U(\omega)$ and have been worked out in [170]. The values of the reduction factor Z_B are between 0.59 and 0.63 for LaFeAsO , FeSe and BaFe_2As_2 [170], which suggests a further enhancement of the effective masses computed by static LDA+DMFT by a factor of at least 1.6 – 1.7 in iron pnictides and raises again the controversy about the precise strength of correlations.

As discussed above, combined DFT+DMFT has been very successful in describing spectral properties of transition metal pnictides, concerning quasi-particle renormalizations, onset of incoherent behavior or even two-particle quantities. Still, quite generally, problems remain concerning the size of the pockets at the Fermi energy: it seems that DFT+DMFT just as the Kohn-Sham band structure of DFT overestimates

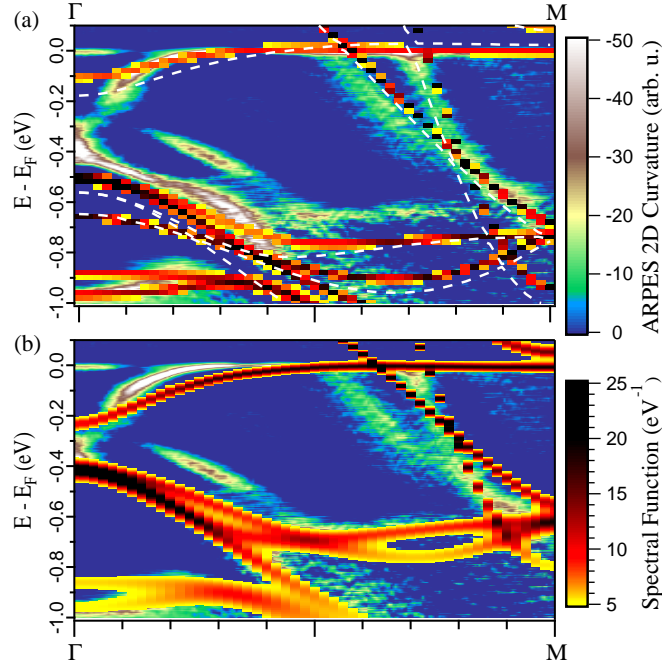


Figure 15: Bands of BaCo₂As₂ along the Γ M direction, extracted from the spectral function calculated by (a) SEx+DDMFT and (b) LDA+DMFT, superimposed on ARPES data from Ref. [46] (represented as a second derivative of the photoemission intensity). The Quasiparticle Self-consistent *GW* band structure is also given (white dashed lines). Reprinted with permission from Ref. [47], copyright ©(2014) by The American Physical Society.

the size of Fermi surface pockets. Since in such calculations the overall particle number fixes the chemical potential self-consistently, an overestimation of hole pockets is necessarily accompanied by an overestimation of electron pockets and vice versa. The additional correction needed is a correction that would be able to “shift the pockets apart”, that is shift hole pockets downwards and electron pocket upwards. In cases, where the pockets are built from different orbital contributions, this would be possible by a purely local but orbital-dependent self-energy correction as provided by local approximation such as DMFT. In the pnictides, however, the requirement is even stricter: *xz/yz* orbitals form both electron and hole pockets, and shifting those apart indicates additional *k*-dependent (that is, nonlocal) corrections. The combined *GW*+DMFT scheme [171, 172, 173, 174, 175] is a promising way to address this challenge. Recently, an even cheaper way has been proposed, namely a scheme that incorporates dynamical screening and non-local exchange into a DMFT calculation [47, 176, 143]. Interestingly, this technique also reconciles the Stoner criterion with the experimental absence of magnetism in BaCo₂As₂. We finish this review by a brief description of these very recent developments.

At the pure *GW* level, it has been found that the self-energy can be roughly separated into a non-local static part and a local – in the sense that it can be expressed in a local basis of Wannier functions – dynamical part at low-energy in the iron pnictides [72] and in the transition metal oxide SrVO₃ [173]. Inspired by this study, one can interpret the non-local static part of the *GW* self-energy as a screened-exchange term, while the dynamical part is attributed to correlations:

$$\Sigma(k, \omega) = \Sigma_{sex}(k) + \Sigma_c(\omega) \quad (19)$$

This corresponds to the application of DMFT on a better starting point than the usual DFT-LDA band structure, that is to say another quasiparticle Hamiltonian H_0 . In [47, 176], Σ_{sex} was approximated by a Hartree-Fock calculation in which the Coulomb potential is replaced by a Yukawa potential defined by the Thomas-Fermi screening length. Σ_c is finally calculated by Dynamical Mean Field Theory, includ-

ing dynamical interactions $U(\omega)$. This technique was dubbed Screened Exchange+Dynamical U DMFT (SEx+DDMFT).

In general, non-local exchange results in an increase of the one-particle bandwidth with respect to LDA, due to the reduced electronic repulsion. On the other hand, the dynamical screening will reduce the bandwidth by the bosonic renormalization factor Z_B discussed above [169, 170, 30]. In BaCo_2As_2 , the combination of those two effects results in a decrease of the spectral weight at the Fermi level with respect to the usual static- U LDA+DMFT calculation. Moreover, the non-local exchange modifies the shape of the Fermi surface, which is primordial in such a compound with a flat band close to the Fermi level (see Figure 15) (and should also be in other pnictides for the prediction of the low-energy properties). This makes the compound fall just below the onset of the Stoner criterion. Similarly to what happens with this weakly-correlated compound, we expect that a more accurate treatment of non-local effects is also needed in other pnictides (including the more correlated ones), in order to achieve a deeper theoretical understanding (and, eventually, a first principles description) of their physical properties.

7. Conclusion

We have reviewed some of the efforts of the last years that have been concerned with the spectral properties of transition metal pnictide compounds. During that period, PES and ARPES (and the preceding sample elaborations that are a prerequisite to reaching good resolution) have reached a mature stage where these techniques can be used to study in some detail quasi-particle excitations and Fermi surfaces in the normal phase, and provide useful information on gap structures in the superconducting phase. At the same time, electronic structure techniques for correlated materials have also tremendously evolved: dynamical mean field theory-based calculations nowadays give quite accurate descriptions of spectral, optical or magnetic properties. Nevertheless, open questions also remain, namely at the interface of electronic structure and many-body theory or concerning the limitations of the local approximation done in DMFT. Due to their incredible sensitivity to tiny changes in the Hund's exchange coupling, iron pnictides are probably a kind of "worst case scenario" for electronic structure calculations, but it is precisely for this reason that the field has made so much progress over the last years: there are few materials classes in nature where such a large number of relatively similar compounds have been studied as intensively as in the field of transition metal pnictides, providing a huge body of benchmark data and putting serious constraints on theoretical modeling.

Acknowledgments

Our view on the field has been shaped by discussions and collaborations with numerous colleagues whom we thank warmly. This work was further supported by supercomputing time at IDRIS/GENCI Orsay, under project 091393, an ERC Consolidator grant (project number 617196), NSF under grant No. NSF PHY11- 25915, grants from MOST (2010CB923000, 2011CBA001000, 2011CBA00102, 2012CB821403 and 2013CB921703) and NSFC (11004232, 11034011/A0402, 11234014 and 11274362) from China, and by the Cai Yuanpei program.

References

- [1] H. Hertz, Ueber einen einfluss des ultravioletten lichtes auf die electrische entladung, *Annalen der Physik* 267 (8) (1887) 983–1000.
- [2] S. Hüfner, *Photoelectron spectroscopy: Principles and applications*, Springer, 2003.
- [3] A. Damascelli, Probing the electronic structure of complex systems by ARPES, *Physica Scripta* 2004 (T109) (2004) 61.
- [4] P. Richard, T. Qian and H. Ding, ARPES measurements of the superconducting gap of Fe-based superconductors and their implications to the pairing mechanism, *J. Phys.: Condens. Matter* 27 (2015) 293203.
- [5] P. Richard, T. Sato, K. Nakayama, T. Takahashi, H. Ding, Fe-based superconductors: an angle-resolved photoemission spectroscopy perspective, *Rep. Prog. Phys.* 74 (12) (2011) 124512.
- [6] J. D. Lee, O. Gunnarsson, L. Hedin, Transition from the adiabatic to the sudden limit in core-level photoemission: A model study of a localized system, *Phys. Rev. B* 60 (1999) 8034–8049.

- [7] L. Hedin, On correlation effects in electron spectroscopies and the *gw* approximation, *Journal of Physics: Condensed Matter* 11 (42) (1999) R489.
- [8] C. Berthod, Many-body Formalism in Condensed Matter Physics, Lecture notes, University of Geneva, 2014.
- [9] J. Braun, J. Minár, H. Ebert, M. I. Katsnelson, A. I. Lichtenstein, Spectral function of ferromagnetic *3d* metals: A self-consistent LSDA + DMFT approach combined with the one-step model of photoemission, *Phys. Rev. Lett.* 97 (2006) 227601.
- [10] J. M. Tomczak, A. I. Poteryaev, S. Biermann, Momentum-resolved spectroscopy of correlated metals: A view from dynamical mean field theory, *Comptes Rendus Physique* 10 (6) (2009) 537–547.
- [11] M. P. Seah, W. A. Dench, Quantitative electron spectroscopy of surfaces: A standard data base for electron inelastic mean free paths in solids, *Surface and Interface Analysis* 1 (1) (1979) 2–11.
- [12] L. Perfetti, P. A. Loukakos, M. Lisowski, U. Bovensiepen, H. Berger, S. Biermann, P. S. Cornaglia, A. Georges, M. Wolf, Time evolution of the electronic structure of *1t-tas₂* through the insulator-metal transition, *Phys. Rev. Lett.* 97 (2006) 067402.
- [13] L. Perfetti, P. A. Loukakos, M. Lisowski, U. Bovensiepen, M. Wolf, H. Berger, S. Biermann, A. Georges, Femtosecond dynamics of electronic states in the Mott insulator *1t-tas₂* by time resolved photoelectron spectroscopy, *New Journal of Physics* 10 (5) (2008) 053019.
- [14] I. Avigo, R. Cortés, L. Rettig, S. Thirupathaiah, H. S. Jeevan, P. Gegenwart, T. Wolf, M. Ligges, M. Wolf, J. Fink, U. Bovensiepen, Coherent excitations and electron-phonon coupling in Ba/EuFe₂As₂ compounds investigated by femtosecond time- and angle-resolved photoemission spectroscopy, *Journal of Physics: Condensed Matter* 25 (9) (2013) 094003.
- [15] L. Rettig, R. Cortés, H. S. Jeevan, P. Gegenwart, T. Wolf, J. Fink, U. Bovensiepen, Electron-phonon coupling in 122 Fe pnictides analyzed by femtosecond time-resolved photoemission, *New Journal of Physics* 15 (8) (2013) 083023.
- [16] D. H. Torchinsky, G. F. Chen, J. L. Luo, N. L. Wang, N. Gedik, Band-dependent quasiparticle dynamics in single crystals of the *ba_{0.6}ko_{0.4}fe₂as₂* superconductor revealed by pump-probe spectroscopy, *Phys. Rev. Lett.* 105 (2010) 027005.
- [17] S. Kumar, L. Harnagea, S. Wurmehl, B. Buchner, A. K. Sood, Ultrafast quasiparticle relaxation dynamics in superconducting iron pnictide Ca(Fe_{0.944}Co_{0.056})₂As₂, *Solid State Communications* 160 (2013) 8 – 12.
- [18] O. Andersen, L. Boeri, On the multi-orbital band structure and itinerant magnetism of iron-based superconductors, *Annalen der Physik* 523 (1-2) (2011) 8–50.
- [19] V. Brouet, M. F. Jensen, P.-H. Lin, A. Taleb-Ibrahimi, P. Le Fèvre, F. Bertran, C.-H. Lin, W. Ku, A. Forget, D. Colson, Impact of the two Fe unit cell on the electronic structure measured by ARPES in iron pnictides, *Phys. Rev. B* 86 (2012) 075123.
- [20] C.-H. Lin, T. Berlijn, L. Wang, C.-C. Lee, W.-G. Yin, W. Ku, One-Fe versus two-Fe Brillouin zone of Fe-based superconductors: Creation of the electron pockets by translational symmetry breaking, *Phys. Rev. Lett.* 107 (2011) 257001.
- [21] W. Kohn, Nobel lecture: Electronic structure of matter—wave functions and density functionals, *Rev. Mod. Phys.* 71 (5) (1999) 1253–1266.
- [22] J. Hubbard, Electron correlations in narrow energy bands, *Proc. R. Soc. London A* 276 (1) (1963) 238.
- [23] J. Hubbard, Electron correlations in narrow energy bands. ii. the degenerate band case, *Proc. R. Soc. London A* 277 (1369) (1964) 237.
- [24] F. Aryasetiawan, M. Imada, A. Georges, G. Kotliar, S. Biermann, A. I. Lichtenstein, Frequency-dependent local interactions and low-energy effective models from electronic structure calculations, *Phys. Rev. B* 70 (19) (2004) 195104.
- [25] L. Vaugier, Electronic structure of correlated materials from first principles: Hubbard interaction and Hund’s exchange, Ph.D. thesis, Ecole Polytechnique, France (2011).
- [26] L. Vaugier, H. Jiang, S. Biermann, Hubbard U and Hund exchange J in transition metal oxides: Screening versus localization trends from constrained random phase approximation, *Phys. Rev. B* 86 (16) (2012) 165105.
- [27] A. van Roekeghem, L. Vaugier, H. Jiang, S. Biermann, Hubbard interactions in iron-based pnictides and chalcogenides: Slater parametrization, screening channels and frequency dependence, In preparation.
- [28] T. Kosugi, T. Miyake, S. Ishibashi, R. Arita, H. Aoki, First-principles electronic structure of solid picene, *Journal of the Physical Society of Japan* 78 (11) (2009) 113704.
- [29] K. Haule and G. Kotliar, *New J. Phys.* 11 (2009) 025021.
- [30] P. Werner, M. Casula, T. Miyake, F. Aryasetiawan, A. J. Millis, S. Biermann, Satellites and large doping- and temperature-dependence of electronic properties in hole-doped BaFe₂As₂, *Nature Physics* 8 (2012) 331–337.
- [31] L. de’ Medici, G. Giovannetti, M. Capone, Selective Mott physics as a key to iron superconductors, *Phys. Rev. Lett.* 112 (2014) 177001.
- [32] S. Biermann, Electronic structure of transition metal compounds: DFT-DMFT approach, in: K. H. J. Buschow, R. W. Cahn, M. C. Flemings, B. I. (print), E. J. Kramer, S. Mahajan, , P. V. (updates) (Eds.), *Encyclopedia of Materials: Science and Technology*, Elsevier, Oxford, 2006, pp. 1 – 9.
- [33] S. Biermann, LDA+DMFT - A tool for investigating the electronic structure of materials with strong electronic coulomb correlations, *Encyclopedia of materials : Science and Technology*.
- [34] A. Georges, G. Kotliar, W. Krauth, M. J. Rozenberg, Dynamical mean-field theory of strongly correlated fermion systems and the limit of infinite dimensions, *Rev. Mod. Phys.* 68 (1) (1996) 13.
- [35] A. Georges, Strongly correlated electron materials: Dynamical mean field theory and electronic structure, *Lectures on the physics of highly correlated electron systems VIII* 715 (2004) 3.
- [36] G. Kotliar, S. Y. Savrasov, K. Haule, V. S. Oudovenko, O. Parcollet, C. A. Marianetti, Electronic structure calculations with dynamical mean-field theory, *Rev. Mod. Phys.* 78 (3) (2006) 865–951.
- [37] R. Bulla, Dynamical mean-field theory - From quantum impurity physics to lattice problems, *Phil. Mag.* 86 (2006) 1877.

- [38] V. I. Anisimov, A. Poteryaev, M. Korotin, A. Anokhin, G. Kotliar, First-principles calculations of the electronic structure and spectra of strongly correlated systems : dynamical mean-field theory, *J. Phys.: Condens. Matter* 9 (1997) 943.
- [39] A. I. Lichtenstein, M. I. Katsnelson, Ab initio calculations of quasiparticle band structure in correlated systems: LDA++ approach, *Phys. Rev. B* 57 (12) (1998) 6884–6895.
- [40] M. Aichhorn, L. Pourovskii, V. Vildosola, M. Ferrero, O. Parcollet, T. Miyake, A. Georges, S. Biermann, Dynamical mean-field theory within an augmented plane-wave framework: Assessing electronic correlations in the iron pnictide LaFeAsO, *Phys. Rev. B* 80 (8) (2009) 085101.
- [41] F. Lechermann, A. Georges, A. Poteryaev, S. Biermann, M. Posternak, A. Yamasaki, O. K. Andersen, Dynamical mean-field theory using wannier functions: A flexible route to electronic structure calculations of strongly correlated materials, *Phys. Rev. B* 74 (12) (2006) 125120.
- [42] M. Ferrero, O. Parcollet, TRIQS: A toolbox for research on interacting quantum systems (2011).
URL <http://ipht.cea.fr/triqs>
- [43] G. D. Mahan, Many-Particle Physics, Plenum Press, New York and London, 1990.
- [44] J. M. Tomczak, S. Biermann, Optical properties of correlated materials: Generalized Peierls approach and its application to VO₂, *Phys. Rev. B* 80 (2009) 085117.
- [45] F. Rullier-Albenque, D. Colson, A. Forget, P. Thuéry, and S. Poissonnet, *Phys. Rev. B* 81 (2010) 224503.
- [46] N. Xu, P. Richard, A. van Roekeghem, P. Zhang, H. Miao, W.-L. Zhang, T. Qian, M. Ferrero, A. S. Sefat, S. Biermann, H. Ding, Electronic band structure of BaCo₂As₂: A fully doped ferropnictide analog with reduced electronic correlations, *Phys. Rev. X* 3 (2013) 011006.
- [47] A. van Roekeghem, T. Ayril, J. M. Tomczak, M. Casula, N. Xu, H. Ding, M. Ferrero, O. Parcollet, H. Jiang, S. Biermann, Dynamical correlations and screened exchange on the experimental bench: spectral properties of the cobalt pnictide BaCo₂As₂, *Phys. Rev. Lett.* 113 (2014) 266403.
- [48] N. Xu, C. E. Matt, P. Richard, A. van Roekeghem, S. Biermann, X. Shi, S.-F. Wu, H.-W. Liu, D. Chen, T. Qian, N. Plumb, M. Radovic, H. Wang, Q. Mao, J. Du, M. Fang, J. Mesot, H. Ding, M. Shi, Camelback-shaped band reconciles heavy electron behavior with weak electronic Coulomb correlations in superconducting TlNi₂Se₂, arXiv:1412.7016.
- [49] K. Haule, J. H. Shim, G. Kotliar, Correlated electronic structure of LaO_{1-x}F_xFeAs, *Phys. Rev. Lett.* 100 (2008) 226402.
- [50] M. Aichhorn, S. Biermann, T. Miyake, A. Georges, M. Imada, Theoretical evidence for strong correlations and incoherent metallic state in FeSe, *Phys. Rev. B* 82 (6) (2010) 064504.
- [51] J. Ferber, K. Foyevtsova, R. Valentí, H. O. Jeschke, LDA+DMFT study of the effects of correlation in LiFeAs, *Phys. Rev. B* 85 (2012) 094505.
- [52] P. Hansmann, R. Arita, A. Toschi, S. Sakai, G. Sangiovanni, K. Held, Dichotomy between large local and small ordered magnetic moments in iron-based superconductors, *Phys. Rev. Lett.* 104 (2010) 197002.
- [53] V. I. Anisimov, D. Korotin, M. Korotin, A. V. Kozhevnikov, J. Kunes, S. A. O., S. L. Skornyakov, S. V. Streltsov, Coulomb repulsion and correlation strength in LaFeAsO from density functional and dynamical mean-field theories, *J. Phys. Condens. Matter* 21 (2009) 075602.
- [54] G. Wang, Y. Qian, G. Xu, X. Dai, Z. Fang, Gutzwiller density functional studies of FeAs-based superconductors: Structure optimization and evidence for a three-dimensional Fermi surface, *Phys. Rev. Lett.* 104 (2010) 047002.
- [55] K. Haule, G. Kotliar, Coherence and incoherence crossover in the normal state of iron oxypnictides and importance of Hund’s rule coupling, *New J. Phys.* 11 (2009) 025021.
- [56] L. de’ Medici, Hund’s coupling and its key role in tuning multiorbital correlations, *Phys. Rev. B* 83 (2011) 205112.
- [57] A. Liebsch, H. Ishida, Correlation-induced spin freezing transition in FeSe: A dynamical mean field study, *Phys. Rev. B* 82 (15) (2010) 155106.
- [58] A. O. Shorikov, M. A. Korotin, S. V. Streltsov, S. L. Skornyakov, D. M. Korotin, V. I. Anisimov, Coulomb correlation effects in LaFeAsO: An LDA+DMFT(QMC) study, *J. Exp. Theor. Phys.* 108 (2009) 121.
- [59] V. I. Anisimov, D. M. Korotin, S. V. Streltsov, A. V. Kozhevnikov, J. Kunes, S. A. O., M. A. Korotin, Density-functional calculation of the coulomb repulsion and correlation strength in superconducting LaFeAsO, *JETP Lett.* 88 (2008) 729.
- [60] T. Miyake, L. Pourovskii, V. Vildosola, S. Biermann, A. Georges, d- and f-orbital correlations in the REFeAsO compounds, *J. Phys. Soc. Jpn. : Supplement C* 77 (2008) 99.
- [61] H. Eschrig, A. Lankau, K. Koepnik, Calculated cleavage behavior and surface states of LaOFeAs, *Phys. Rev. B* 81 (2010) 155447.
- [62] L. X. Yang, B. P. Xie, Y. Zhang, C. He, Q. Q. Ge, X. F. Wang, X. H. Chen, M. Arita, J. Jiang, K. Shimada, M. Taniguchi, I. Vobornik, G. Rossi, J. P. Hu, D. H. Lu, Z. X. Shen, Z. Y. Lu, D. L. Feng, Surface and bulk electronic structures of LaFeAsO studied by angle-resolved photoemission spectroscopy, *Phys. Rev. B* 82 (2010) 104519.
- [63] C. Liu, Y. Lee, A. D. Palczewski, J.-Q. Yan, T. Kondo, B. N. Harmon, R. W. McCallum, T. A. Lograsso and A. Kaminski, *Phys. Rev. B* 82 (2010) 075135.
- [64] D. Hsieh, Y. Xia, L. Wray, D. Qian, K. Gomes, A. Yazdani, G. Chen, J. Luo, N. Wang, M. Hasan, Experimental determination of the microscopic origin of magnetism in parent iron pnictides, arXiv:0812.2289.
- [65] D. Lu, M. Yi, S.-K. Mo, J. Analytis, J.-H. Chu, A. Erickson, D. Singh, Z. Hussain, T. Geballe, I. Fisher, Z.-X. Shen, ARPES studies of the electronic structure of LaOFe(P,As), *Physica C* 469 (9-12) (2009) 452–458.
- [66] E. van Heumen, J. Vuorinen, K. Koepnik, F. Massee, Y. Huang, M. Shi, J. Klei, J. Goedkoop, M. Lindroos, J. van den Brink and M. S. Golden, *Phys. Rev. Lett.* 106 (2011) 027002.
- [67] S. Wu, P. Richard, A. van Roekeghem, S. M. Nie, H. Miao, N. Xu, T. Qian, B. Saparov, Z. Fang, S. Biermann, A. S. Sefat, H. Ding, Direct spectroscopic evidence for completely filled cu 3d shell in BaCu₂As₂ and α -BaCu₂Sb₂, *Phys. Rev. B* 91 (2015) 235109.
- [68] A. Yamasaki, Y. Matsui, S. Imada, K. Takase, H. Azuma, T. Muro, Y. Kato, A. Higashiya, A. Sekiyama, S. Suga,

- M. Yabashi, K. Tamasaku, T. Ishikawa, K. Terashima, H. Kobori, A. Sugimura, N. Umeyama, H. Sato, Y. Hara, N. Miyagawa, S. I. Ikeda, Electron correlation in the FeSe superconductor studied by bulk-sensitive photoemission spectroscopy, *Phys. Rev. B* 82 (2010) 184511.
- [69] D. Lu, M. Yi, S.-K. Mo, A. Erickson, J. Analytis, J.-H. Chu, D. Singh, Z. Hussain, T. Geballe, I. Fisher, Z. Shen, Electronic structure of the iron-based superconductor LaOFeP, *Nature* 455 (7209) (2008) 81–84.
- [70] R. Yoshida, T. Wakita, H. Okazaki, Y. Mizuguchi, S. Tsuda, Y. Takano, H. Takeya, K. Hirata, T. Muro, M. Okawa, K. Ishizaka, S. Shin, H. Harima, M. Hirai, Y. Muraoka, T. Yokoya, Electronic structure of superconducting FeSe studied by high-resolution photoemission spectroscopy, *J. Phys. Soc. Jpn.* 78 (2009) 034708.
- [71] S. V. Borisenko, V. B. Zabolotnyy, D. V. Evtushinsky, T. K. Kim, I. V. Morozov, A. N. Yaresko, A. A. Kordyuk, G. Behr, A. Vasiliev, R. Follath, B. Büchner, Superconductivity without nesting in LiFeAs, *Phys. Rev. Lett.* 105 (2010) 067002.
- [72] J. M. Tomczak, M. van Schilfgaarde, G. Kotliar, Many-body effects in iron pnictides and chalcogenides: Nonlocal versus dynamic origin of effective masses, *Phys. Rev. Lett.* 109 (2012) 237010.
- [73] H. Ding, P. Richard, K. Nakayama, K. Sugawara, T. Arakane, Y. Sekiba, A. Takayama, S. Souma, T. Sato, T. Takahashi, Z. Wang, X. Dai, Z. Fang, G. F. Chen, J. L. Luo, N. L. Wang, Observation of Fermi-surface-dependent nodeless superconducting gaps in $\text{Ba}_{0.6}\text{K}_{0.4}\text{Fe}_2\text{As}_2$, *EPL* 83 (4) (2008) 47001.
- [74] C. Liu, G. D. Samolyuk, Y. Lee, N. Ni, T. Kondo, A. F. Santander-Syro, S. L. Bud'ko, J. L. McChesney, E. Rotenberg, T. Valla, A. V. Fedorov, P. C. Canfield, B. N. Harmon, A. Kaminski, K-doping dependence of the Fermi surface of the iron-arsenic $\text{Ba}_{1-x}\text{K}_x\text{Fe}_2\text{As}_2$ superconductor using angle-resolved photoemission spectroscopy, *Phys. Rev. Lett.* 101 (2008) 177005.
- [75] V. Brouet, M. Marsi, B. Mansart, A. Nicolaou, A. Taleb-Ibrahimi, P. Le Fèvre, F. Bertran, F. Rullier-Albenque, A. Forget, D. Colson, Nesting between hole and electron pockets in $\text{Ba}(\text{Fe}_{1-x}\text{Co}_x)_2\text{As}_2$ ($x = 0 - 0.3$) observed with angle-resolved photoemission, *Phys. Rev. B* 80 (2009) 165115.
- [76] T. Shimojima, K. Ishizaka, Y. Ishida, N. Katayama, K. Ohgushi, T. Kiss, M. Okawa, T. Togashi, X.-Y. Wang, C.-T. Chen, S. Watanabe, R. Kadota, T. Oguchi, A. Chainani, S. Shin, Orbital-dependent modifications of electronic structure across the magnetostructural transition in BaFe_2As_2 , *Phys. Rev. Lett.* 104 (2010) 057002.
- [77] S. de Jong, Y. Huang, R. Huisman, F. Massee, S. Thirupathaiah, M. Gorgoi, F. Schaefer, R. Follath, J. B. Goedkoop, M. S. Golden, High-resolution, hard x-ray photoemission investigation of BaFe_2As_2 : Moderate influence of the surface and evidence for a low degree of Fe $3d$ -As $4p$ hybridization of electronic states near the Fermi energy, *Phys. Rev. B* 79 (2009) 115125.
- [78] J. Fink, S. Thirupathaiah, R. Ovsyannikov, H. A. Dürr, R. Follath, Y. Huang, S. de Jong, M. S. Golden, Y.-Z. Zhang, H. O. Jeschke, R. Valentí, C. Felser, S. Dastjani Farahani, M. Rotter, D. Johrendt, Electronic structure studies of BaFe_2As_2 by angle-resolved photoemission spectroscopy, *Phys. Rev. B* 79 (2009) 155118.
- [79] W. Malaeb, T. Yoshida, A. Fujimori, M. Kubota, K. Ono, K. Kihou, P. M. Shirage, H. Kito, A. Iyo, H. Eisaki, Y. Nakajima, T. Tamegai, R. Arita, Three-dimensional electronic structure of superconducting iron pnictides observed by angle-resolved photoemission spectroscopy, *J. Phys. Soc. Jpn.* 78 (12) (2009) 123706.
- [80] D. J. Singh, Electronic structure of Fe-based superconductors, *Physica C* 469 (9) (2009) 418–424.
- [81] V. Vildosola, L. Pourovskii, R. Arita, S. Biermann, A. Georges, Bandwidth and Fermi surface of iron oxypnictides: Covalency and sensitivity to structural changes, *Phys. Rev. B* 78 (2008) 064518.
- [82] I. I. Mazin, D. J. Singh, M. D. Johannes, M. H. Du, Unconventional superconductivity with a sign reversal in the order parameter of $\text{LaFeAsO}_{1-x}\text{F}_x$, *Phys. Rev. Lett.* 101 (2008) 057003.
- [83] V. Brouet, P.-H. Lin, Y. Texier, J. Bobroff, A. Taleb-Ibrahimi, P. Le Fèvre, F. Bertran, M. Casula, P. Werner, S. Biermann, F. Rullier-Albenque, A. Forget, D. Colson, Large temperature dependence of the number of carriers in Co-doped BaFe_2As_2 , *Phys. Rev. Lett.* 110 (2013) 167002.
- [84] C. Liu, T. Kondo, A. Palczewski, G. Samolyuk, L. Y., M. Tillman, N. Ni, E. Mun, R. Gordon, A. Santander-Syro, S. Bud'ko, J. McChesney, E. Rotenberg, A. Fedorov, T. Valla, O. Copie, M. Tanatar, C. Martin, B. Harmon, P. Canfield, R. Prozorov, J. Schmalian, A. Kaminski, Electronic properties of iron arsenic high temperature superconductors revealed by angle resolved photoemission spectroscopy (ARPES), *Physica C* 469 (9-12) (2009) 491–497.
- [85] P. Vilmercati, A. Fedorov, I. Vobornik, U. Manju, G. Panaccione, A. Goldoni, A. S. Sefat, M. A. McGuire, B. C. Sales, R. Jin, D. Mandrus, D. J. Singh, N. Mannella, Evidence for three-dimensional Fermi-surface topology of the layered electron-doped iron superconductor $\text{Ba}(\text{Fe}_{1-x}\text{Co}_x)_2\text{As}_2$, *Phys. Rev. B* 79 (2009) 220503.
- [86] I. I. Mazin, M. D. Johannes, L. Boeri, K. Koepernik, D. J. Singh, Problems with reconciling density functional theory calculations with experiment in ferropnictides, *Phys. Rev. B* 78 (2008) 085104.
- [87] M. Aichhorn, L. Pourovskii, A. Georges, Importance of electronic correlations for structural and magnetic properties of the iron pnictide superconductor LaFeAsO , *Phys. Rev. B* 84 (2011) 054529.
- [88] G. Lee, H. S. Ji, Y. Kim, C. Kim, K. Haule, G. Kotliar, B. Lee, S. Khim, K. H. Kim, K. S. Kim, K.-S. Kim, J. H. Shim, Orbital selective Fermi surface shifts and mechanism of high T_c superconductivity in correlated AFeAs ($A=\text{Li}, \text{Na}$), *Phys. Rev. Lett.* 109 (2012) 177001.
- [89] H. Ding, K. Nakayama, P. Richard, S. Souma, T. Sato, T. Takahashi, M. Neupane, Y.-M. Xu, Z.-H. Pan, A. V. Fedorov, Z. Wang, X. Dai, Z. Fang, G. F. Chen, J. L. Luo, N. L. Wang, Electronic structure of optimally doped pnictide $\text{Ba}_{0.6}\text{K}_{0.4}\text{Fe}_2\text{As}_2$: A comprehensive angle-resolved photoemission spectroscopy investigation, *J. Phys. Condens. Matter* 23 (13) (2011) 135701.
- [90] Y. Lubashevsky, E. Lahoud, K. Chashka, D. Podolsky and A. Kanigel, *Nature Phys.* 8 (2012) 309.
- [91] J. Malet, V. B. Zabolotnyy, D. V. Evtushinsky, S. Thirupathaiah, A. U. B. Wolter, L. Harnagea, A. N. Yaresko, A. N. Vasiliev, D. A. Chareev, A. E. Böhmer, F. Hardy, T. Wolf, C. Meingast, E. D. L. Rienks, B. Büchner, S. V. Borisenko, Unusual band renormalization in the simplest iron-based superconductor FeSe_{1-x} , *Phys. Rev. B* 89 (2014) 220506.

- [92] K. Nakayama, Y. Miyata, G. N. Phan, T. Sato, Y. Tanabe, T. Urata, K. Tanigaki, T. Takahashi, Reconstruction of band structure induced by electronic nematicity in an FeSe superconductor, *Phys. Rev. Lett.* 113 (2014) 237001.
- [93] T. Shimojima, Y. Suzuki, T. Sonobe, A. Nakamura, M. Sakano, J. Omachi, K. Yoshioka, M. Kuwata-Gonokami, K. Ono, H. Kumigashira, A. E. Böhrer, F. Hardy, T. Wolf, C. Meingast, H. v. Löhneysen, H. Ikeda, K. Ishizaka, Lifting of xz / yz orbital degeneracy at the structural transition in detwinned FeSe, *Phys. Rev. B* 90 (2014) 121111.
- [94] K. Okazaki, Y. Ito, Y. Ota, Y. Kotani, T. Shimojima, T. Kiss, S. Watanabe, C.-T. Chen, S. Niitaka, T. Hanaguri, H. Takagi, A. Chainani, S. Shin, Superconductivity in an electron band just above the fermi level: possible route to BCS-BEC superconductivity, *Scientific reports* 4.
- [95] S. Kasahara, T. Watashige, T. Hanaguri, Y. Kohsaka, T. Yamashita, Y. Shimoyama, Y. Mizukami, R. Endo, H. Ikeda, K. Aoyama, et al., Field-induced superconducting phase of FeSe in the BCS-BEC cross-over, *Proceedings of the National Academy of Sciences* 111 (46) (2014) 16309–16313.
- [96] M. D. Watson, T. K. Kim, A. A. Haghighirad, N. R. Davies, A. McCollam, A. Narayanan, S. F. Blake, Y. L. Chen, S. Ghannadzadeh, A. J. Schofield, M. Hoesch, C. Meingast, T. Wolf, A. I. Coldea, Emergence of the nematic electronic state in FeSe, *Phys. Rev. B* 91 (2015) 155106.
- [97] P. Zhang, T. Qian, P. Richard, X. P. Wang, H. Miao, B. Q. Lv, B. B. Fu, T. Wolf, C. Meingast, X. X. Wu, Z. Q. Wang, J. P. Hu, H. Ding, Observation of two distinct d_{xz}/d_{yz} band splittings in FeSe, *Phys. Rev. B* 91 (2015) 214503.
- [98] Y. Suzuki, T. Shimojima, T. Sonobe, A. Nakamura, M. Sakano, H. Tsuji, J. Omachi, K. Yoshioka, M. Kuwata-Gonokami, T. Watashige, R. Kobayashi, S. Kasahara, T. Shibauchi, Y. Matsuda, Y. Yamakawa, H. Kontani, K. Ishizaka, Momentum-dependent sign-inversion of orbital polarization in superconducting FeSe, *arXiv:1504.00980*.
- [99] Y. Zhang, M. Yi, Z.-K. Liu, W. Li, J. J. Lee, R. G. Moore, M. Hashimoto, N. Masamichi, H. Eisaki, S.-K. Mo, Z. Hussain, T. P. Devereaux, Z.-X. Shen, D. H. Lu, Distinctive momentum dependence of the band reconstruction in the nematic state of FeSe thin film, *arXiv:1503.01556*.
- [100] K. Umezawa, Y. Li, H. Miao, K. Nakayama, Z.-H. Liu, P. Richard, T. Sato, J. B. He, D.-M. Wang, G. F. Chen, H. Ding, T. Takahashi and S.-C. Wang, *Phys. Rev. Lett.* 108 (2012) 037002.
- [101] S. V. Borisenko, V. B. Zabolotnyy, A. A. Kordyuk, D. V. Evtushinsky, T. K. Kim, I. V. Morozov, R. Follath and B. Büchner, *Symmetry* 4 (2012) 251.
- [102] S. Chi, S. Johnston, G. Levy, S. Grothe, R. Szedlak, B. Ludbrook, R. Liang, P. Dosanjh, S. A. Burke, A. Damascelli, D. A. Bonn, W. N. Hardy, Y. Pennec, Sign inversion in the superconducting order parameter of LiFeAs inferred from Bogoliubov quasiparticle interference, *Phys. Rev. B* 89 (2014) 104522.
- [103] M. van Schilfgaarde, T. Kotani, S. Faleev, Quasiparticle self-consistent GW theory, *Phys. Rev. Lett.* 96 (22) (2006) 226402.
- [104] D. J. Singh, Electronic structure and doping in BaFe₂As₂ and LiFeAs: Density functional calculations, *Phys. Rev. B* 78 (2008) 094511.
- [105] S. Borisenko, D. Evtushinsky, I. Morozov, S. Wurmehl, B. Büchner, A. Yaresko, T. Kim, M. Hoesch, T. Wolf, N. Zhigadlo, Direct observation of spin-orbit coupling in iron-based superconductors, *arXiv: 1409.8669*.
- [106] M. Yi, D. H. Lu, J. G. Analytis, J.-H. Chu, S.-K. Mo, R.-H. He, R. G. Moore, X. J. Zhou, G. F. Chen, J. L. Luo, N. L. Wang, Z. Hussain, D. J. Singh, I. R. Fisher, Z.-X. Shen, Electronic structure of the BaFe₂As₂ family of iron-pnictide superconductors, *Phys. Rev. B* 80 (2009) 024515.
- [107] A. Tamai, A. Y. Ganin, E. Rozbicki, J. Bacsá, W. Meevasana, P. D. C. King, M. Caffio, R. Schaub, S. Margadonna, K. Prassides, M. J. Rosseinsky, F. Baumberger, Strong electron correlations in the normal state of the iron-based FeSe_{0.42}Te_{0.58} superconductor observed by angle-resolved photoemission spectroscopy, *Phys. Rev. Lett.* 104 (2010) 097002.
- [108] C. He, Y. Zhang, B. P. Xie, X. F. Wang, L. X. Yang, B. Zhou, F. Chen, M. Arita, K. Shimada, H. Namatame, M. Taniguchi, X. H. Chen, J. P. Hu, D. L. Feng, Electronic-structure-driven magnetic and structure transitions in superconducting NaFeAs single crystals measured by angle-resolved photoemission spectroscopy, *Phys. Rev. Lett.* 105 (2010) 117002.
- [109] S. T. Cui, S. Y. Zhu, A. F. Wang, S. Kong, S. L. Ju, X. G. Luo, X. H. Chen, G. B. Zhang, Z. Sun, Evolution of the band structure of superconducting NaFeAs from optimally doped to heavily overdoped Co substitution using angle-resolved photoemission spectroscopy, *Phys. Rev. B* 86 (2012) 155143.
- [110] V. Brouet, F. Rullier-Albenque, M. Marsi, B. Mansart, M. Aichhorn, S. Biermann, J. Faure, L. Perfetti, A. Taleb-Ibrahimi, P. Le Fèvre, F. Bertran, A. Forget, D. Colson, Significant reduction of electronic correlations upon isovalent Ru substitution of BaFe₂As₂, *Phys. Rev. Lett.* 105 (2010) 087001.
- [111] N. Xu, T. Qian, P. Richard, Y.-B. Shi, X.-P. Wang, P. Zhang, Y.-B. Huang, Y.-M. Xu, H. Miao, G. Xu, G.-F. Xuan, W.-H. Jiao, Z.-A. Xu, G.-H. Cao, H. Ding, Effects of Ru substitution on electron correlations and Fermi-surface dimensionality in Ba(Fe_{1-x}Ru_x)₂As₂, *Phys. Rev. B* 86 (2012) 064505.
- [112] T. Sato, K. Nakayama, Y. Sekiba, P. Richard, Y.-M. Xu, S. Souma, T. Takahashi, G. F. Chen, J. L. Luo, N. L. Wang, H. Ding, Band structure and Fermi surface of an extremely overdoped iron-based superconductor KFe₂As₂, *Phys. Rev. Lett.* 103 (2009) 047002.
- [113] T. Yoshida, S.-I. Ideta, I. Nishi, A. Fujimori, M. Yi, R. Moore, S.-K. Mo, D. Lu, Z.-X. Shen, Z. Hussain, et al., Orbital character and electron correlation effects on two- and three-dimensional Fermi surfaces in KFe₂As₂ revealed by angle-resolved photoemission spectroscopy, *Frontiers in Physics* 2 (2014) 17.
- [114] A. Kordyuk, V. Zabolotnyy, D. Evtushinsky, A. Yaresko, B. Büchner, S. Borisenko, Electronic band structure of ferro-pnictide superconductors from ARPES experiment, *Journal of superconductivity and novel magnetism* 26 (9) (2013) 2837–2841.
- [115] E. Razzoli, C. E. Matt, M. Kobayashi, X.-P. Wang, V. N. Strocov, A. van Roekeghem, S. Biermann, N. C. Plumb,

- M. Radovic, T. Schmitt, C. Capan, Z. Fisk, P. Richard, H. Ding, P. Aebi, J. Mesot, M. Shi, Tuning electronic correlations in transition metal pnictides: Chemistry beyond the valence count, *Phys. Rev. B* 91 (2015) 214502.
- [116] K. Terashima, Y. Sekiba, J. H. Bowen, K. Nakayama, T. Kawahara, T. Sato, P. Richard, Y.-M. Xu, L. J. Li, G. H. Cao, Z.-A. Xu, H. Ding and T. Takahashi, *Proc. Natl. Acad. Sci. USA* 106 (2009) 7330.
- [117] V. Brouet, M. F. Jensen, A. Nicolaou, A. Taleb-Ibrahimi, P. L. Fèvre, F. Bertran, A. Forget, D. Colson, Orbitaly resolved lifetimes in $\text{Ba}(\text{Fe}_{0.92}\text{Co}_{0.08})_2\text{As}_2$ measured by ARPES, *Phys. Rev. B* 85 (2012) 144508.
- [118] F. Chen, B. Zhou, Y. Zhang, J. Wei, H.-W. Ou, J.-F. Zhao, C. He, Q.-Q. Ge, M. Arita, K. Shimada, H. Namatame, M. Taniguchi, Z.-Y. Lu, J. Hu, X.-Y. Cui, D. L. Feng, Electronic structure of $\text{Fe}_{1.04}\text{Te}_{0.66}\text{Se}_{0.34}$, *Phys. Rev. B* 81 (2010) 014526.
- [119] K. Nakayama, T. Sato, P. Richard, T. Kawahara, Y. Sekiba, T. Qian, G. F. Chen, J. L. Luo, N. L. Wang, H. Ding, T. Takahashi, Angle-resolved photoemission spectroscopy of the iron-chalcogenide superconductor $\text{Fe}_{1.03}\text{Te}_{0.7}\text{Se}_{0.3}$: Strong coupling behavior and the universality of interband scattering, *Phys. Rev. Lett.* 105 (2010) 197001.
- [120] T. Hajiri, T. Ito, R. Niwa, M. Matsunami, B. H. Min, Y. S. Kwon, S. Kimura, Three-dimensional electronic structure and interband nesting in the stoichiometric superconductor LiFeAs , *Phys. Rev. B* 85 (2012) 094509.
- [121] M. Yi, D. H. Lu, R. G. Moore, K. Kihou, C.-H. Lee, A. Iyo, H. Eisaki, T. Yoshida, A. Fujimori and Z.-X. Shen, *New J. Phys.* 14 (2012) 073019.
- [122] Z. R. Ye, Y. Zhang, F. Chen, M. Xu, J. Jiang, X. H. Niu, C. H. P. Wen, L. Y. Xing, X. C. Wang, C. Q. Jin, B. P. Xie, D. L. Feng, Extraordinary doping effects on quasiparticle scattering and bandwidth in iron-based superconductors, *Phys. Rev. X* 4 (2014) 031041.
- [123] W. Malaeb, T. Yoshida, T. Kataoka, A. Fujimori, M. Kubota, K. Ono, H. Usui, K. Kuroki, R. Arita, H. Aoki, et al., Electronic structure and electron correlation in $\text{LaFeAsO}_{1-x}\text{F}_x$ and $\text{LaFePO}_{1-x}\text{F}_x$, *Journal of the Physical Society of Japan* 77 (9) (2008) 093714.
- [124] I. Nishi, M. Ishikado, S. Ideta, W. Malaeb, T. Yoshida, A. Fujimori, Y. Kotani, M. Kubota, K. Ono, M. Yi, D. H. Lu, R. Moore, Z.-X. Shen, A. Iyo, K. Kihou, H. Kito, H. Eisaki, S. Shamoto and R. Arita, *Phys. Rev. B* 84 (2011) 014504.
- [125] W. Malaeb, T. Yoshida, A. Fujimori, M. Kubota, K. Ono, K. Kihou, P. M. Shirage, H. Kito, A. Iyo, H. Eisaki, Y. Nakajima, T. Tamegai, R. Arita, Three-dimensional electronic structure of superconducting iron pnictides observed by angle-resolved photoemission spectroscopy, *J. Phys. Soc. Jpn.* 78 (2008) 123706.
- [126] Y. Zhang, F. Chen, C. He, B. Zhou, B. P. Xie, C. Fang, W. F. Tsai, X. H. Chen, H. Hayashi, J. Jiang, H. Iwasawa, K. Shimada, H. Namatame, M. Taniguchi, J. P. Hu, D. L. Feng, Orbital characters of bands in the iron-based superconductor $\text{BaFe}_{1.85}\text{Co}_{0.15}\text{As}_2$, *Phys. Rev. B* 83 (2011) 054510.
- [127] R. S. Dhaka, Y. Lee, V. K. Anand, D. C. Johnston, B. N. Harmon, A. Kaminski, Angle-resolved photoemission spectroscopy study of BaCo_2As_2 , *Phys. Rev. B* 87 (2013) 214516.
- [128] S. Thirupathaiah, S. de Jong, R. Ovsyannikov, H. A. Dürr, A. Varykhalov, R. Follath, Y. Huang, R. Huisman, M. S. Golden, Y.-Z. Zhang, H. O. Jeschke, R. Valentí, A. Erb, A. Gloskovskii, J. Fink, Orbital character variation of the Fermi surface and doping dependent changes of the dimensionality in $\text{BaFe}_{2-x}\text{Co}_x\text{As}_2$ from angle-resolved photoemission spectroscopy, *Phys. Rev. B* 81 (2010) 104512.
- [129] M. Yi, D. H. Lu, R. Yu, S. C. Riggs, J.-H. Chu, B. Lv, Z. K. Liu, M. Lu, Y.-T. Cui, M. Hashimoto, S.-K. Mo, Z. Hussain, C. W. Chu, I. R. Fisher, Q. Si, Z.-X. Shen, Observation of temperature-induced crossover to an orbital-selective Mott phase in $\text{A}_x\text{Fe}_{2-y}\text{Se}_2$ ($\text{A}=\text{K}, \text{Rb}$) superconductors, *Phys. Rev. Lett.* 110 (2013) 067003.
- [130] L. de' Medici, S. R. Hassan, M. Capone, X. Dai, Orbital-selective Mott transition out of band degeneracy lifting, *Phys. Rev. Lett.* 102 (2009) 126401.
- [131] N. Lanatà, H. U. R. Strand, G. Giovannetti, B. Hellsing, L. de' Medici, M. Capone, Orbital selectivity in hund's metals: The iron chalcogenides, *Phys. Rev. B* 87 (2013) 045122.
- [132] E. Ieki, K. Nakayama, Y. Miyata, T. Sato, H. Miao, N. Xu, X.-P. Wang, P. Zhang, T. Qian, P. Richard, Z.-J. Xu, J. S. Wen, G. D. Gu, H. Q. Luo, H.-H. Wen, H. Ding, T. Takahashi, Evolution from incoherent to coherent electronic states and its implications for superconductivity in $\text{FeTe}_{1-x}\text{Se}_x$, *Phys. Rev. B* 89 (2014) 140506.
- [133] M. H. Fang, H. M. Pham, B. Qian, T. J. Liu, E. K. Vehstedt, Y. Liu, L. Spinu, Z. Q. Mao, Superconductivity close to magnetic instability in $\text{Fe}(\text{Se}_{1-x}\text{Te}_x)_{0.82}$, *Phys. Rev. B* 78 (2008) 224503.
- [134] T. Liu, J. Hu, B. Qian, D. Fobes, Z. Mao, W. Bao, M. Reehuis, S. Kimber, K. Prokeš, S. Matas, D. Argyriou, A. Hiess, A. Rotaru, H. Pham, L. Spinu, Y. Qiu, V. Thampy, A. Savici, J. Rodriguez, C. Broholm, From $(\pi, 0)$ magnetic order to superconductivity with (π, π) magnetic resonance in $\text{Fe}_{1.02}\text{Te}_{1-x}\text{Se}_x$, *Nat. Mater.* 9 (9) (2010) 718–720.
- [135] Y. Mizuguchi, Y. Takano, Review of Fe chalcogenides as the simplest Fe-based superconductor, *J. Phys. Soc. Jpn* 79 (10) (2010) 102001.
- [136] P. Werner, E. Gull, M. Troyer, A. J. Millis, Spin freezing transition and non-Fermi-liquid self-energy in a three-orbital model, *Phys. Rev. Lett.* 101 (16) (2008) 166405.
- [137] Y. Nomura, S. Sakai, R. Arita, Nonlocal correlations induced by hund's coupling: A cluster dmft study, *Phys. Rev. B* 91 (2015) 235107.
- [138] C. Aron, G. Kotliar, Analytic theory of hund's metals: A renormalization group perspective, *Phys. Rev. B* 91 (2015) 041110.
- [139] P.-H. Lin, Y. Texier, A. Taleb-Ibrahimi, P. Le Fèvre, F. Bertran, E. Giannini, M. Grioni, V. Brouet, Nature of the bad metallic behavior of $\text{Fe}_{1.06}\text{Te}$ inferred from its evolution in the magnetic state, *Phys. Rev. Lett.* 111 (2013) 217002.
- [140] Y.-M. Xu, P. Richard, K. Nakayama, T. Kawahara, Y. Sekiba, T. Qian, M. Neupane, S. Souma, T. Sato, T. Takahashi, H.-Q. Luo, H.-H. Wen, G.-F. Chen, N.-L. Wang, Z. Wang, Z. Fang, X. Dai, H. Ding, Fermi surface dichotomy of the superconducting gap and pseudogap in underdoped pnictides, *Nat. Commun.* 2 (2011) 394.
- [141] T. Misawa, K. Nakamura, M. Imada, *Ab Initio* evidence for strong correlation associated with mott proximity in iron-

- based superconductors, *Phys. Rev. Lett.* 108 (2012) 177007.
- [142] L. de' Medici, J. Mravlje, A. Georges, Janus-faced influence of Hund's rule coupling in strongly correlated materials, *Phys. Rev. Lett.* 107 (2011) 256401.
 - [143] A. van Roekeghem, P. Richard, X. Shi, S.-F. Wu, L.-K. Zeng, B. I. Saparov, Y. Ohtsubo, T. Qian, A. Safa-Sefat, S. Biermann, H. Ding, Tetragonal and collapsed-tetragonal phases of CaFe_2As_2 – a view from angle-resolved photoemission and dynamical mean field theory, arXiv:1505.00753.
 - [144] H. Ding, P. Richard, K. Nakayama, K. Sugawara, T. Arakane, Y. Sekiba, A. Takayama, S. Souma, T. Sato, T. Takahashi, Z. Wang, X. Dai, Z. Fang, G. F. Chen, J. L. Luo and N. L. Wang, *Europhys. Lett.* 83 (2008) 47001.
 - [145] L. Zhao, H.-Y. Liu, W.-T. Zhang, J.-Q. Meng, X.-W. Jia, G.-D. Liu, X.-Li Dong, G.-F. Chen, J.-L. Luo, N.-L. Wang, W. Lu, G.-L. Wang, Y. Zhou, Y. Zhu, X.-Y. Wang, Z.-Y. Xu, C.-T. Chen and X.-J. Zhou, *Chin. Phys. Lett.* 25 (2008) 4402.
 - [146] T. Kondo, A. F. Santander-Syro, O. Copie, C. Liu, M. E. Tillman, E. D. Mun, J. Schmalian, S. L. Bud'ko, M. A. Tanatar, P. C. Canfield, A. Kaminski, Momentum dependence of the superconducting gap in $\text{NdFeAsO}_{0.9}\text{F}_{0.1}$ single crystals measured by angle resolved photoemission spectroscopy, *Phys. Rev. Lett.* 101 (2008) 147003.
 - [147] Z.-H. Liu, P. Richard, K. Nakayama, G.-F. Chen, S. Dong, J.-B. He, D.-M. Wang, T.-L. Xia, K. Umezawa, T. Kawahara, S. Souma, T. Sato, T. Takahashi, T. Qian, Y. Huang, N. Xu, Y. Shi, H. Ding, S.-C. Wang, Unconventional superconducting gap in $\text{NaFe}_{0.95}\text{Co}_{0.05}\text{As}$ observed by angle-resolved photoemission spectroscopy, *Phys. Rev. B* 84 (2011) 064519.
 - [148] I. I. Mazin, D. J. Singh, M. D. Johannes, M. H. Du, Unconventional superconductivity with a sign reversal in the order parameter of $\text{LaFeAsO}_{1-x}\text{F}_x$, *Phys. Rev. Lett.* 101 (2008) 057003.
 - [149] I. I. Mazin and J. Schmalian, *Physica C* 469 (2009) 614.
 - [150] K. Kuroki, S. Onari, R. Arita, H. Usui, Y. Tanaka, H. Kontani, H. Aoki, Unconventional pairing originating from the disconnected fermi surfaces of superconducting $\text{LaFeAsO}_{1-x}\text{F}_x$, *Phys. Rev. Lett.* 101 (2008) 087004.
 - [151] S. Graser, T. A. Maier, P. J. Hirschfeld and D. J. Scalapino, *N. J. Phys.* 11 (2009) 025016.
 - [152] V. Cvetkovic and Z. Tesanovic, *Europhys. Lett.* 85 (2009) 37002.
 - [153] K. Nakayama, T. Sato, P. Richard, Y.-M. Xu, Y. Sekiba, S. Souma, G. F. Chen, J. L. Luo, N. L. Wang, H. Ding and T. Takahashi, *Europhys. Lett.* 85 (2009) 67002.
 - [154] J. Guo, S. Jin, G. Wang, S. Wang, K. Zhu, T. Zhou, M. He and X. Chen, *Phys. Rev. B* 82 (2010) 180520(R).
 - [155] M.-H. Fang, H.-D. Wang, C.-H. Dong, Z.-J. Li, C.-M. Feng, J. Chen and H. Q. Yuan, *Europhys. Lett.* 94 (2011) 27009.
 - [156] T. Qian, X.-P. Wang, W.-C. Jin, P. Zhang, P. Richard, G. Xu, X. Dai, Z. Fang, J.-G. Guo, X.-L. Chen and H. Ding, *Phys. Rev. Lett.* 106 (2011) 187001.
 - [157] X.-P. Wang, T. Qian, P. Richard, P. Zhang, J. Dong, H.-D. Wang, C.-H. Dong, M.-H. Fang and H. Ding, *Europhys. Lett.* 93 (2011) 57001.
 - [158] D. Mou, S. Liu, X. Jia, J. He, Y. Peng, Lin Zhao, L. Yu, G. Liu, S. He, X. Dong, J. Zhang, H. Wang, C. Dong, M. Fang, X. Wang, Q. Peng, Z. Wang, S. Zhang, F. Yang, Z. Xu, C. Chen, and X. J. Zhou, *Phys. Rev. Lett.* 106 (2011) 107001.
 - [159] Y. Zhang, L. X. Yang, M. Xu, Z. R. Ye, F. Chen, C. He, H. C. Xu, J. Jiang, B. P. Xie, J. J. Ying, X. F. Wang, X. H. Chen, J. P. Hu, M. Matsunami, S. Kimura and D. L. Feng, *Nature Mater.* 10 (2011) 273.
 - [160] X.-P. Wang, P. Richard, X. Shi, A. Roekeghem, Y.-B. Huang, E. Razzoli, T. Qian, E. Rienks, S. Thirupathaiah, H.-D. Wang, C.-H. Dong, M.-H. Fang, M. Shi and H. Ding, *Europhys. Lett.* 99 (2012) 67001.
 - [161] T. Sato, K. Nakayama, Y. Sekiba, P. Richard, Y.-M. Xu, S. Souma, T. Takahashi, G. F. Chen, J. L. Luo, N. L. Wang and H. Ding, *Phys. Rev. Lett.* 103 (2009) 047002.
 - [162] T. Yoshida, I. Nishi, A. Fujimori, M. Yi, R. G. Moore, D.-H. Lu, Z.-X. Shen, K. Kihou, P. M. Shirage, H. Kito, C. H. Lee, A. Iyo, H. Eisaki and H. Harima, *J. Chem. Phys. Sol.* 72 (2011) 465.
 - [163] J. Hu, H. Ding, *Sci. Rep.* 2 (2012) 381.
 - [164] A. N. Yaresko, G.-Q. Liu, V. N. Antonov, O. K. Andersen, Interplay between magnetic properties and Fermi surface nesting in iron pnictides, *Phys. Rev. B* 79 (2009) 144421.
 - [165] H. Miao, P. Richard, Y. Tanaka, K. Nakayama, T. Qian, K. Umezawa, T. Sato, Y.-M. Xu, Y.-B. Shi, N. Xu, X.-P. Wang, P. Zhang, H.-B. Yang, Z.-J. Xu, J. S. Wen, G.-D. Gu, X. Dai, J.-P. Hu, T. Takahashi and H. Ding, *Phys. Rev. B* 85 (2012) 094506.
 - [166] Z. P. Yin, K. Haule and G. Kotliar, *Nature Phys.* 10 (2014) 845.
 - [167] X. Lu, C. Fang, W.-F. Tsai, Y. Jiang and J. Hu, *Phys. Rev. B* 85 (2012) 054505.
 - [168] P. Zhang, P. Richard, T. Qian, X. Shi, J. Ma, L.-K. Zeng, X.-P. Wang, E. Rienks, C.-L. Zhang, P. Dai, Y.-Z. You, Z.-Y. Weng, X.-X. Wu, J. P. Hu and H. Ding, *Phys. Rev. X* 4 (2014) 0310001.
 - [169] M. Casula, A. Rubtsov, S. Biermann, Dynamical screening effects in correlated materials: Plasmon satellites and spectral weight transfers from a Green's function ansatz to extended dynamical mean field theory, *Phys. Rev. B* 85 (2012) 035115.
 - [170] M. Casula, P. Werner, L. Vaugier, F. Aryasetiawan, T. Miyake, A. J. Millis, S. Biermann, Low-energy models for correlated materials: Bandwidth renormalization from coulombic screening, *Phys. Rev. Lett.* 109 (2012) 126408.
 - [171] S. Biermann, F. Aryasetiawan, A. Georges, First-principles approach to the electronic structure of strongly correlated systems: Combining the GW Approximation and Dynamical Mean-Field Theory, *Phys. Rev. Lett.* 90 (8) (2003) 086402.
 - [172] J. M. Tomczak, M. Casula, T. Miyake, F. Aryasetiawan, S. Biermann, Combined GW and dynamical mean-field theory: Dynamical screening effects in transition metal oxides, *EPL* 100 (6) (2012) 67001.
 - [173] J. M. Tomczak, M. Casula, T. Miyake, S. Biermann, Asymmetry in band widening and quasiparticle lifetimes in SrVO_3 : Competition between screened exchange and local correlations from combined GW and dynamical mean-field theory GW + DMFT, *Phys. Rev. B* 90 (2014) 165138.
 - [174] T. Ayral, P. Werner, S. Biermann, Spectral properties of correlated materials: Local vertex and nonlocal two-particle correlations from combined GW and dynamical mean field theory, *Phys. Rev. Lett.* 109 (2012) 226401.

- [175] T. Ayral, S. Biermann, P. Werner, Screening and nonlocal correlations in the extended Hubbard model from self-consistent combined GW and dynamical mean field theory, *Phys. Rev. B* 87 (2013) 125149.
- [176] A. van Roekeghem, S. Biermann, Screened exchange dynamical mean-field theory and its relation to density functional theory: SrVO_3 and SrTiO_3 , *EPL* 108 (2014) 75003.